CAMS Solar radiation products Regular Validation Report, Issue #32, Sept.-Nov. 2020

Mireille Lefèvre

HAL Id: hal-03621889
https://minesparis-psl.hal.science/hal-03621889

Submitted on 28 Mar 2022

Copernicus Atmosphere Monitoring Service

D72.1.3.1
Regular Validation Report
Issue #32
S-O-N 2020

CAMS-72
Solar radiation products

Issued by: Armines / M. Lefèvre

Date: 28/05/2021

Ref: CAMS72_2018SC2_D72.1.3.1-2021Q2_RAD_validation_report_SON2020_v1

Contributors

ARMINES
Mireille Lefèvre

Table of Contents

Executive summary

The CRS is continuously monitored against ground-based irradiance observations. This includes stations in various geographical locations and climates (see maps in Fig. 2.1 and description in section 4.2). Several stations being affected by large satellite viewing angles are included by intention to provide quantitative insight where the CRS may become unreliable for some applications (Tab. 2.1). From the last #31 issue onwards, a new table of the ground datasets performance is presented with the amount of data rejected / retained for each station by the quality check (Tab. 2.2).

From #30 issue onwards, the protocol of validation (see Annex A.5) has been changed regarding the threshold applied for the usable measurements. For the consistency, the same new protocol has been applied to every SON quarter in the multi-annual plots.

In this #32 issue, two BSRN stations, Budapest in Europe, and Reunion Island with a tropical climate have been added.

For SON 2020, the correlation is very good for global (*G*, Fig. 3.4), good for beam irradiances *(B*, Fig. 3.6) and diffuse (*D*, Fig. 3.5) except stations Florianopolis, Oujda and Cairo, stations with suspicious measurements (see section 4.4). It should be noted that all stations with low satellite viewing have good performance for *G*, *D* and *B* except Florianopolis (with unusual discrepancies measurements in September). Regarding the clearness indices, the beam KT_B are at the same level as for *B* for all stations. The global KT_G and diffuse KT_D correlations are lower than those for *G* and *D* for all stations. They give good performances for global KT_G with the weakest value (0.75) for Reunion Island, but poor performance for diffuse KT_D except Gobabeb and Fki-Ben-Salah (>0.80).

The bias for the global irradiance is null or low for 17 stations and noticeable or large for 14 stations out of 31 (Tab. 3.1). In term of relative absolute value, the bias is <= 6 % for all stations except Missour with -9 % (Fig. 3.1).
At all stations the lowest CRS clearness index KT_G < 0.1 and the highest KT_G in range [0.7, 0.9] are under-represented at the benefit of KT_G in medium range [0.2, 0.6] (Fig. 3.8), i.e., KT_G is overestimated for low values and underestimated for high values. The same scheme can be observed on the irradiances (Fig. 3.7). For stations with low KT_G (frequent cloudy skies) lowest *G* in range [0, 50] W m^{-2} are overestimated to the range [50, 150] W m^{-2}. For stations with frequent clear skies, *G* is well distributed with a slight underestimation of the highest *G* >= 800 W m^{-2}. The multi-annual indicators highlight a better performance for this SON quarter in 2020 compared to previous years (Fig. 3.16b).

The bias for the diffuse irradiance (Fig. 3.2) is null or low for 15 stations out of 19, and noticeable or large for 4 stations: Florianopolis, Missour, Cairo and Izaña. The frequency distributions

([Fig. 3.10](#)) of the KT$_D$ < 0.1 and KT$_D$ > 0.3 are clearly under-represented for the benefit of *KT$_D$* in the range [0.1, 0.3], i.e., low *D* are always overestimated, which is more impacting for stations with strong cloudy skies. Only Izaña, at a high altitude, exhibits a correct frequency distribution for the low KT$_D$ but frequent clear skies along with an under-representation of higher values leads to a noticeable negative bias. The same dynamics is reproduced with irradiances ([Fig. 3.9](#)). For stations with frequent cloudy skies the low *D* < 50 W m^{-2} are overestimated to range [50, 150] W m^{-2} while for stations with frequent clear skies, low *D* < 100 W m^{-2} are overestimated to range [100, 300] W m^{-2}. For all stations, *D* > 300 W m^{-2} are underestimated.

Such as G, the multi-annual indicators ([Fig. 3.17b](#)) show similar or better results for SON 2020 compared to previous years, except for Florianopolis (with unusual measurements discrepancies in September) and Izaña, at a high altitude.

The bias for the direct normal irradiances ([Fig. 3.3](#)) is good but larger for the stations of Florianopolis, Missour and Fki-Ben-Salah. For stations with frequent cloudy skies, the frequency distributions ([Fig. 3.12](#)) of KT$_B$ < 0.1 are slightly under-represented for the benefit of *KT$_B$* in the range [0.1, 0.3]. For stations with frequent clear skies, the KT$_B$ > 0.6 are under-represented for the benefit of range [0.1, 0.4]. The frequency distribution of irradiances ([Fig. 3.11](#)) follows the same dynamics. For stations with frequent cloudy skies, lowest *B* < 50 W m^{-2} are overestimated to range [100, 400] W m^{-2}. For stations with frequent clear skies, highest *B* > 700 W m^{-2} are underestimated to range [100, 700] W m^{-2} except for Fki-Ben-Salah.

Such as *G* and *D*, the multi-annual indicators ([Fig. 3.18b](#)) show similar or better results for SON 2020 compared to previous years, except for Florianopolis (with unusual measurements discrepancies in September), Izaña and Fki-Ben-Salah.

The monthly means of the estimated *G* ([Fig. 3.13](#)) are identical or close to those of the measurements at all stations. In desertic climates *G* is slightly underestimated while it is slightly overestimated or similar in other regions. The monthly standard deviations that highlight the dynamics of the dataset are slightly underestimated at most stations.

For *D* ([Fig. 3.14](#)) the discrepancies rely overall on the lower dynamics of the estimated values compared to measurements. That was illustrated with the frequency distributions.

The monthly means of the estimated *B* ([Fig. 3.15](#)) are slightly underestimated or close to measurements at most stations, with standard deviations slightly lower. The exceptions to this rule are stations above cited for their bad results: Florianopolis, Fki-Ben-Salah overestimate both the monthly mean and the standard deviation, Cairo and Izaña overestimate the monthly mean.

As a whole, the frequency distributions of measurements of hourly means, expressed as binned histograms, are not well represented by CRS, although correlations are quite good. For the 3 components, a loss of dynamics is generally observed for the estimated values compared to measurements. This loss is slight for *G* and concerns mainly stations with frequent cloudy skies; it is higher for *D* and *B*. For the stations with frequent cloudy skies, the frequency of the lowest irradiances is too low (irradiances are overestimated, or clouds not well detected). For the stations

with frequent clear skies, the frequency of the highest irradiances is too low (irradiances are underestimated, or clouds detected when there are absent). That is in accordance with the frequent observations of low monthly standard deviations mentioned above.

Stations with low satellite viewing angle give good results. Among them, Kauno and Silutes have beneficiated of a renovation at the beginning of 2020 and CRS estimation exhibits from then much better results.
The stations Gobabeb, in desert climate, and Izaña, with a high altitude (2373 m) present a good frequency distribution of KT_G along with good performance for the G correlation, bias and RSME. Contrary to Gobabeb, Izaña have weak results for D and B.
The enerMENA stations of Fki-Ben-Salah, Cairo, Missour and Oujda give weak results at least on one component. This could be due to the frequent deposition of particulate matter in these desertic regions together with frequent problems of maintenance (see Table 2.1 and section 4.4). Apart these stations, SON 2020 give weak results on station Florianopolis which presents some unusual discrepancies in measurements in Sept. 2020 (section 4.4.5).
The new station of Budapest shows very good results for the 3 components, although the frequency distribution is in line with the overall performance. The new station of Reunion Island, in tropical climate, give results in line with the overall performance.

At most stations the multi-annual indicators show similar or better results for SON 2020 compared to previous years. Although straddled on two IFS cycles (CY46r1 for Sept. and CY47r1 for Oct.-Nov.) the impact of CY47r1 on SON 2020 is clearly positive.

1 Introduction

The CAMS Radiation Service, abbreviated as CRS, delivers estimates of the solar radiation arriving at ground level on a horizontal surface. Outcomes of the CRS have to be validated on a periodic basis. Following practices in CAMS, this validation is performed every quarter. Following current practices, the CRS irradiances are tested against qualified ground measurements measured at several ground-based stations serving as reference. These ground measurements are coincident in time with the CRS estimates.
This report is issue #32 of a regular report performed with version 3 of the CRS. It deals with hourly means of global, diffuse, and direct irradiances for the period Sept.-Oct. -Nov. 2020, abbreviated as SON 2020.

In #24 of this report a multi-annual assessment was introduced for each station as a 3-years times-series in Annex C. This assessment is provided once a year for the yyyyQ3 report (DJF datasets) when in-situ measurements are completed for the year. This has made the quarterly validation reports very large. Therefore, from issue #25 onwards detailed results are partly provided in a zip archive supplement as individual files in a well-organized folder structure.

From #27 (2019Q3 report) onwards, multi-annual statistical indicators of the respective season are given in section 3.

From #31 (2021Q1 report) onwards, a summary of the quality check operated on each station is given in section 2.

The results discussed in this report may also be retrieved for several of the selected stations and others by running the service "Irradiation Validation Report" on the SoDa website: http://www.soda-pro.com/fr/web-services/validation/irradiation-validation-report . This service "Irradiation Validation Report" performs a comparison of the hourly or daily solar irradiation at surface estimated by the CRS against several qualified ground measurements obtained from various sources. It returns a HTML page that contains statistics of comparisons and graphs. Similar calculations can be done for the estimates of solar radiation from the HelioClim-3 databases, allowing comparisons with the CRS.

2 Stations

The source of ground-based measurements is given in section 4, along with a description of each station and the products provided: *G*, *B*, *D* are global, beam and diffuse irradiances respectively, and KT_G, KT_B, KT_D are global, beam and diffuse clearness indices, respectively. These parameters are defined in Annex A.7.

2.1 Maps

Figure 2.1 shows the location of the stations as reported in Table 4.2. Symbols code the initial summarization of the data as reported in Table 4.1: circle for 1 min, and downward triangle for 1 h. Colors code the type of data at each site: red for (*G, B, D*), yellow for (*G, B*), magenta for (*G, D*) and cyan for *G*.

In the #27 report, some stations have been removed from the set of usual stations, and some others have been added (see Fig. 2.3 in #27). Stations too close to the sea like Hoorn (see 4.1.1 in #27 for the report of the problem) and Vlissingen in the Netherlands have been removed and replaced by Leeuwarden and Maastricht (Fig. 2.3). Stations have been closed by the providers like Carpentras and Dobele in December 2018, Rucava in September 2018, or are not updated regularly like PSA (year 2017 was provisioned in December 2018, years 2018 and 2019 was provisioned in April 2020). New stations offset these removals like CENER in Spain, or Aluksne and Kolka, two new stations provided monthly by the Latvian network instead of Dobele and Rucava. Since November 2019, the enerMENA network provides a new station Fki-Ben-Salah in Morocco. In the #31 report, the KNMI station of Cabauw has been replaced with the same station provided by the BSRN network that offers the 3 components *G*, *D* and *B* at 1 min of resolution. The BSRN station of Izaña has been added for evaluation at a high altitude. In this #32 report, the BSRN stations of Budapest and Reunion Island have been added.
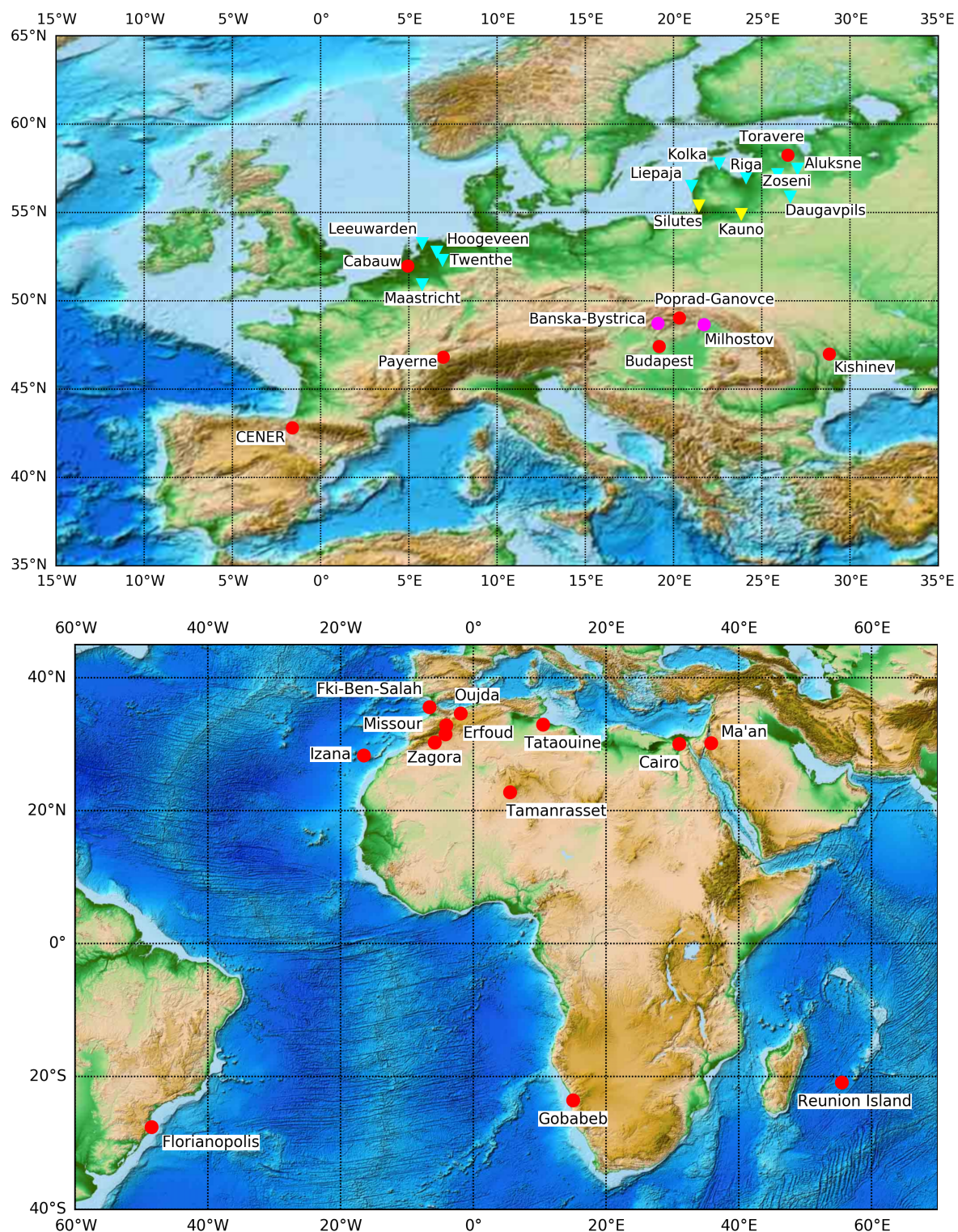
Figure 2.1. Maps showing the 21 stations in Europe (top) and 13 stations outside Europe (bottom). Symbols code the initial summarization: circle for 1 min, and downward triangle for 1 h. Colors code the type of data at each site: red for (*G, B, D*), yellow for (*G, B*), magenta for (*G, D*) and cyan for *G*.

2.2 List of the stations retained for this quarter

Depending on the provision of fresh data, possible problems affecting measuring instruments, possible rejection of some data by the quality control, and other causes, it is not always possible to use the same set of stations to perform the quarterly validation. Table 2.1 lists the 32 stations that have been retained for this quarter, along with the 2 stations usually retained but having no available data for this quarter.

Due to low satellite viewing angles, lower CRS quality is expected for stations in Lettland and Lithuania (Aluksne, Daugavpils, Kauno, Kolka, Liepaja, Riga, Silutes, Toravere) and Brazil (Florianopolis). Nevertheless, stations in Lettland and Lithuania provide some insight on the area where the CRS may become unreliable and therefore, this information is kept in this user-oriented report. The same reason motivates the new addition of Izaña at a high altitude.

A summary of the quality check operated on each station is given in Table 2.2 ([section 2.3](#)).

Table 2.1. List of stations retained or excluded for this regular validation report.

Station	Variables	Issues for the period
Aluksne	G - -	Reduced service accuracy expected due to low satellite viewing angle.
Banska-Bystrica	G D -	
Budapest	G D B	**New BSRN station.**
Cabauw	G D B	From issue #31 onwards, the KNMI dataset with 1 h resolution and only G component is replaced with the BSRN dataset offering 1 min resolution and the 3 components.
Cairo	G D B	Only Sept. Tracking failure in Oct.-Nov.
CENER	G D B	
Daugavpils	G - -	Reduced service accuracy expected due to low satellite viewing angle.
Erfoud	G D B	Good quality.
Florianopolis	G D B	Reduced service accuracy expected due to low satellite viewing angle.
Fki-Ben-Salah	- D B	*D* data good quality. *G* data not available due to broken sensor. Pyrheliometer sometimes in the afternoon misaligned due to mounting error. *B* mounting enhanced and anemometer repaired during maintenance visit on Nov 19th, 2020. Cleaning button broken.
Gobabeb	G D B	
Hoogeveen	G - -	
Izaña	G D B	New station to be evaluated for regular validation. Reduced service accuracy expected due to altitude 2372 m.
Kauno	G - B	Reduced service accuracy expected due to low satellite viewing angle.
Kishinev	G D B	

Station	Variables	Issues for the period
Kolka	G - -	Reduced service accuracy expected due to low satellite viewing angle.
Leeuwarden	G - -	
Liepaja	G - -	Reduced service accuracy expected due to low satellite viewing angle.
Ma'an	G D B	Tracker unaligned at first hour during the day. Data gap between Oct. 15th and Nov. 1st 2020. Cleaning every ~4 days.
Maastricht	G - -	
Milhostov	G D -	
Missour	G D B	Good quality, but many short data gaps due to power failures of the logger. Cleaning every ~1-2 days. Data gap between Nov. 14th and end of Nov. 2020 due to logger failure.
Oujda	G D B	Good quality, but several tracker outages. Cleaning every ~3 days
Payerne	G D B	**No data available from February 2020 onwards**.
Poprad-Ganovce	G D B	
Reunion Island	G D B	**New BSRN station.**
Riga	G - -	Reduced service accuracy expected due to low satellite viewing angle.
Silutes	G - B	Reduced service accuracy expected due to low satellite viewing angle.
Tamanrasset	G D B	Only *G* is available. *D* and *B* unavailable from March 2018 onwards.
Tataouine	G D B	Good quality, cleaning every ~3days.
Toravere	G D B	**No data available from June 2020 onwards.** Reduced service accuracy expected due to low satellite viewing angle.
Twenthe	G - -	
Zagora	G D B	Good quality.
Zoseni	G - -	Reduced service accuracy expected due to low satellite viewing angle.

2.3 Quality check

Table 2.2 summarizes for each station:

- The number of usable values in the ground dataset expressed as a percentage of the number of daylight instants in the SON period, i.e., the number of instants corresponding to the source resolution (1 h or 1 min) for a solar zenith angle SZA <= 89°.

- The number of values rejected by the quality check (QC) expressed as a percentage of the usable values in the ground dataset.

- The number of retained values in the ground dataset after the quality check, expressed as a percentage of the number of daylight instants in the SON 2020 period. That represents the dimension of the ground dataset before the summarization to hourly resolution and the application of the SZA threshold.

Table 2.2. Quantities of ground measurements rejected or retained for each station in SON 2020 period.

Station	Variable	Daylight instants during SON 2020	Observation >=0 during daylight before QC		QC Test	Data rejected by the QC during daylight		Observation >=0 during daylight after QC and before SZA threshold	
		N	N	%		N	%	N	%
Aluksne	G	895	895	100.0	BSRN-1C	0	0.000	895	100.0
Banska-Bystrica	G	57006	56967	99.9	BSRN-2C	3	0.005	56931	99.9
	D		56942	99.9		8	0.014	56931	99.9
Budapest	G	57382	57382	100.0	BSRN-3C	189	0.329	56355	98.2
	D		57382	100.0		191	0.333	56355	98.2
	B		56531	98.5		170	0.301	56355	98.2
CENER	G	58547	58356	99.7	BSRN-3C	69	0.118	55430	94.7
	D		58353	99.7		65	0.111	55430	94.7
	B		55531	94.8		57	0.103	55430	94.7
Cabauw	G	55951	55725	99.6	BSRN-3C	32	0.057	55205	98.7
	D		55700	99.6		49	0.088	55205	98.7
	B		55595	99.4		28	0.050	55205	98.7
Cairo	G	60993	11096	18.2	BSRN-3C	0	0.000	10742	17.6
	D		11062	18.1		6	0.054	10742	17.6
	B		10775	17.7		5	0.046	10737	17.6
Daugavpils	G	906	904	99.8	BSRN-1C	0	0.000	904	99.8
Erfoud	G	60744	60208	99.1	BSRN-3C	1	0.002	60206	99.1
	D		60208	99.1		0	0.000	60206	99.1
	B		60353	99.4		0	0.000	60206	99.1
Fki-Ben-Salah	D	60554	59283	97.9	BSRN-1C	0	0.000	59283	97.9
	B		59556	98.4		0	0.000	59556	98.4
Florianopolis	G	67996	67919	99.9	BSRN-3C	40	0.059	65952	97.0
	D		67854	99.8		1374	2.025	65952	97.0
	B		67395	99.1		33	0.049	65952	97.0
Gobabeb	G	67450	67145	99.5	BSRN-3C	37	0.055	66997	99.3
	D		67396	99.9		38	0.056	66997	99.3
	B		67376	99.9		21	0.031	66997	99.3
Hoogeveen	G	928	928	100.0	BSRN-1C	0	0.000	928	100.0
Izaña	G	61247	59545	97.2	BSRN-3C	5	0.008	55840	91.2
	D		56506	92.3		3	0.005	55840	91.2
	B		56180	91.7		0	0.000	55840	91.2
Kauno	G	916	916	100.0	BSRN-1C	1	0.109	915	99.9
	B		916	100.0		14	1.528	902	98.5

Station	Variable	Daylight instants during SON 2020	Observation >=0 during daylight before QC		QC Test	Data rejected by the QC during daylight		Observation >=0 during daylight after QC and before SZA threshold	
		N	N	%		N	%	N	%
Kishinev	G	951	951	100.0	BSRN-3C	14	1.472	936	98.4
	D		951	100.0		14	1.472	936	98.4
	B		951	100.0		28	2.944	923	97.1
Kolka	G	892	892	100.0	BSRN-1C	1	0.112	891	99.9
Leeuwarden	G	923	923	100.0	BSRN-1C	0	0.000	923	100.0
Liepaja	G	904	904	100.0	BSRN-1C	1	0.111	903	99.9
Ma'an	G	60980	46913	76.9	BSRN-3C	45	0.096	46860	76.8
	D		46910	76.9		48	0.102	46860	76.8
	B		46975	77.0		45	0.096	46860	76.8
Maastricht	G	943	943	100.0	BSRN-1C	0	0.000	943	100.0
Milhostov	G	57035	57029	100.0	BSRN-2C	0	0.000	56983	99.9
	D		56996	99.9		13	0.023	56983	99.9
Missour	G	60516	16640	27.5	BSRN-3C	7	0.042	16625	27.5
	D		16632	27.5		6	0.036	16625	27.5
	B		16657	27.5		6	0.036	16625	27.5
Oujda	G	60205	58787	97.6	BSRN-3C	26	0.044	54105	89.9
	D		54374	90.3		219	0.403	54105	89.9
	B		59077	98.1		26	0.044	54105	89.9
Poprad-Ganovce	G	56922	56907	100.0	BSRN-3C	495	0.870	54200	95.2
	D		56875	99.9		505	0.888	54200	95.2
	B		54718	96.1		484	0.885	54200	95.2
Riga	G	899	899	100.0	BSRN-1C	1	0.111	898	99.9
Réunion Island	G	67111	67082	100.0	BSRN-3C	181	0.270	66410	99.0
	D		67094	100.0		181	0.270	66410	99.0
	B		66616	99.3		180	0.270	66410	99.0
Silutes	G	910	910	100.0	BSRN-1C	0	0.000	910	100.0
	B		910	100.0		15	1.648	895	98.4
Tamanrasset	G	62046	61201	98.6	BSRN-1C	0	0.000	61201	98.6
Tataouine	G	60502	56528	93.4	BSRN-3C	2	0.004	56524	93.4
	D		56535	93.4		2	0.004	56524	93.4
	B		56574	93.5		2	0.004	56524	93.4
Twenthe	G	932	932	100.0	BSRN-1C	0	0.000	932	100.0
Zagora	G	60942	60295	98.9	BSRN-3C	1	0.002	60294	98.9
	D		60296	98.9		0	0.000	60294	98.9

Station	Variable	Daylight instants during SON 2020	Observation >=0 during daylight before QC		QC Test	Data rejected by the QC during daylight		Observation >=0 during daylight after QC and before SZA threshold	
		N	N	%		N	%	N	%
Zoseni	B		60482	99.2	BSRN-1C	0	0.000	60294	98.9
	GI	898	898	100.0		0	0.000	898	100.0

3 Overview of the results

Following the ISO standard (1995), the deviations are computed by subtracting observations for each instant from the product estimations (CRS - measurements), and are summarized by usual statistical quantities such as the bias or the root mean square error. The validation procedure is described in Annex A. Detailed results for the report's season are given for each station in Annexes B.

3.1 Bias and standard deviation of errors

Detailed tables for the SON 2020 quarter summarize the performance of the CRS for hourly means of global irradiance (in W m^{-2}, Tab. 3.1), corresponding clearness index (Tab. 3.2), and the performances relative to the mean of measurements (in percent, Tab. 3.3). Similar detailed tables are given for the D component (Tab. 3.4 to 3.6) and the B component (Tab. 3.7 to 3.9). They are available as an excel file in a folder of the supplemental zip archive:

CAMS72_2018SC2_D72.1.3.1-2021Q2_section3_statistical_metrics/
CAMS72_2018SC2_D72.1.3.1-2021Q2_section3_statistical_metrics_SON2020.xlsx

Table 3.1 summarizes the performance of CRS for the hourly mean of irradiances. The following empirical rules adopted for the bias are derived from the uncertainty (20 W m^{-2}) of the measurements of hourly irradiation of good quality from the recommendations of the WMO (see Annex A, Table A.1).

Table 3.1. Number of stations in each category of bias (in W m^{-2})

Rules for the bias (in W m^{-2})		G	D
Null bias	Absolute value of the bias ≤ 5	7	11
Low bias	5 < absolute value of the bias ≤ 10	10	4
Noticeable bias	10 < absolute value of the bias ≤ 20	9	3
Large bias	20 < absolute value of the bias ≤ 60	5	1
Very large bias	Absolute value of the bias > 60	0	0
Number of stations		31	19

Relative biases and RMSE are given in Figures 3.1, 3.2 and 3.3 for respectively *G*, *D* and *B*.
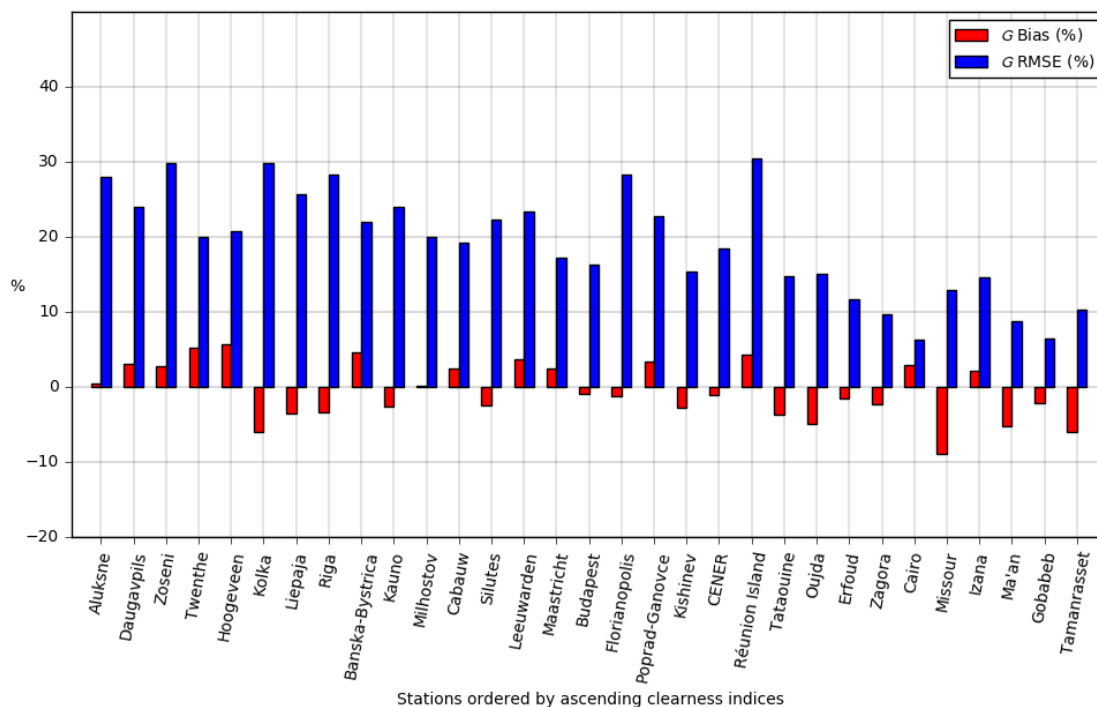
Figure 3.1. Relative bias and RMSE for global irradiance.
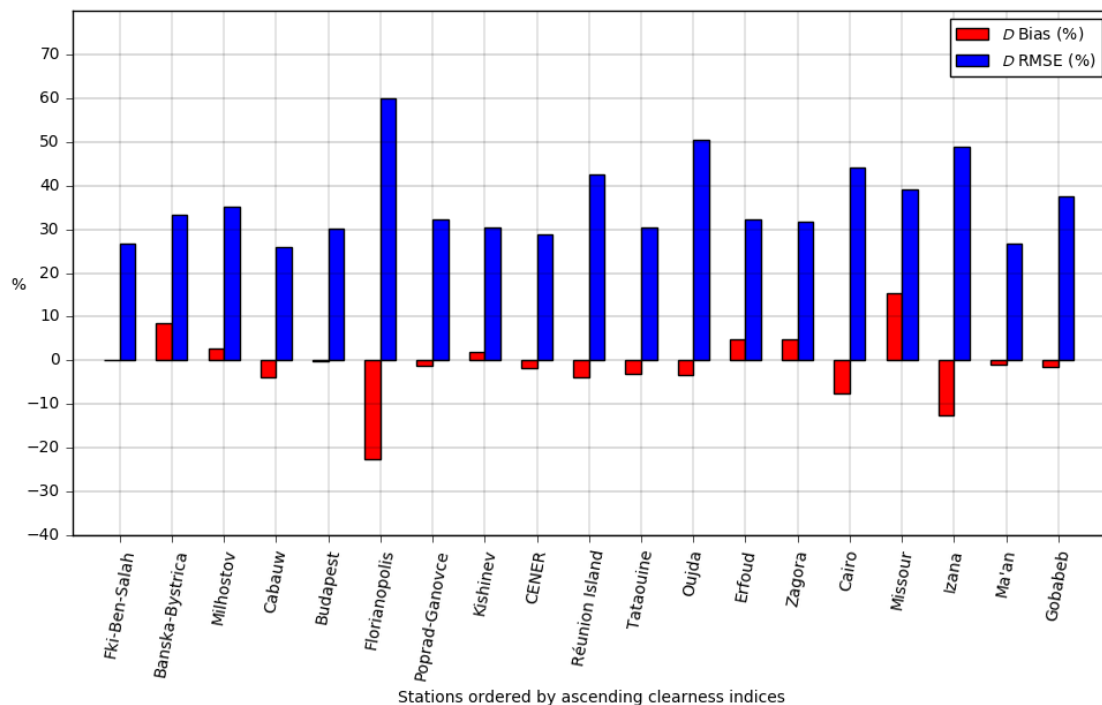
Figure 3.2. Relative bias and RMSE for diffuse irradiance.
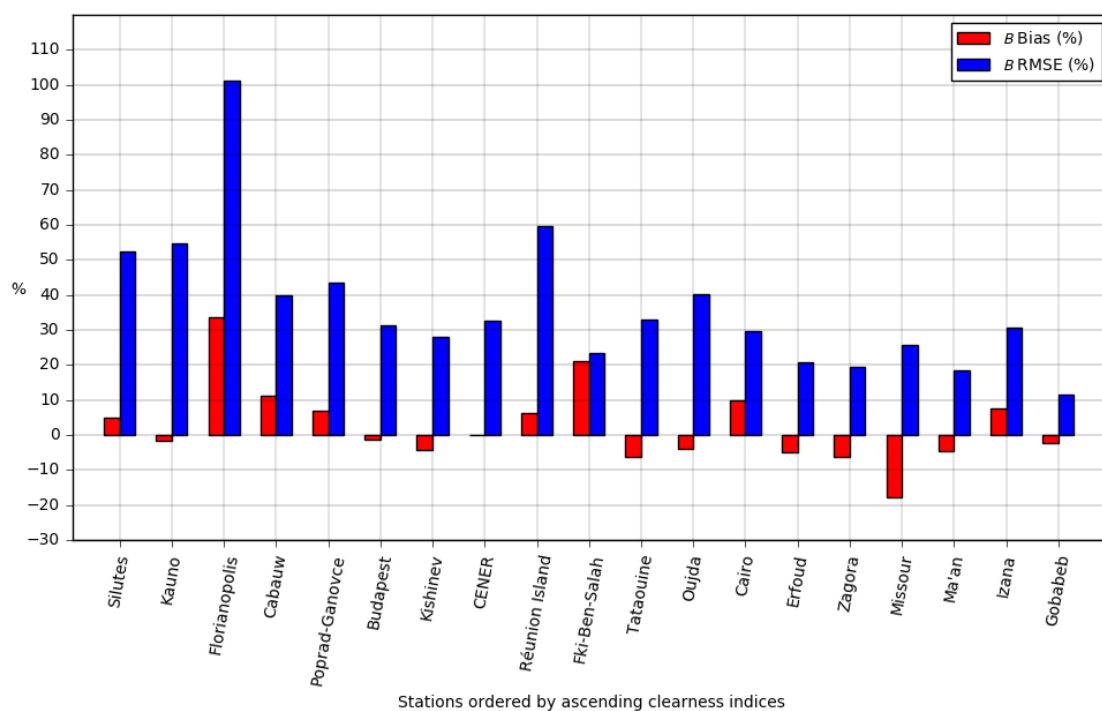
Figure 3.3. Relative bias and RMSE for direct irradiance.

3.2 Ability to reproduce the intra-day variability

The correlation coefficients of the SON 2020 quarter are displayed for irradiances and clearness indices: G and KT_G (Fig. 3.4), D and KT_D (Fig. 3.5), B and KT_B (Fig. 3.6).
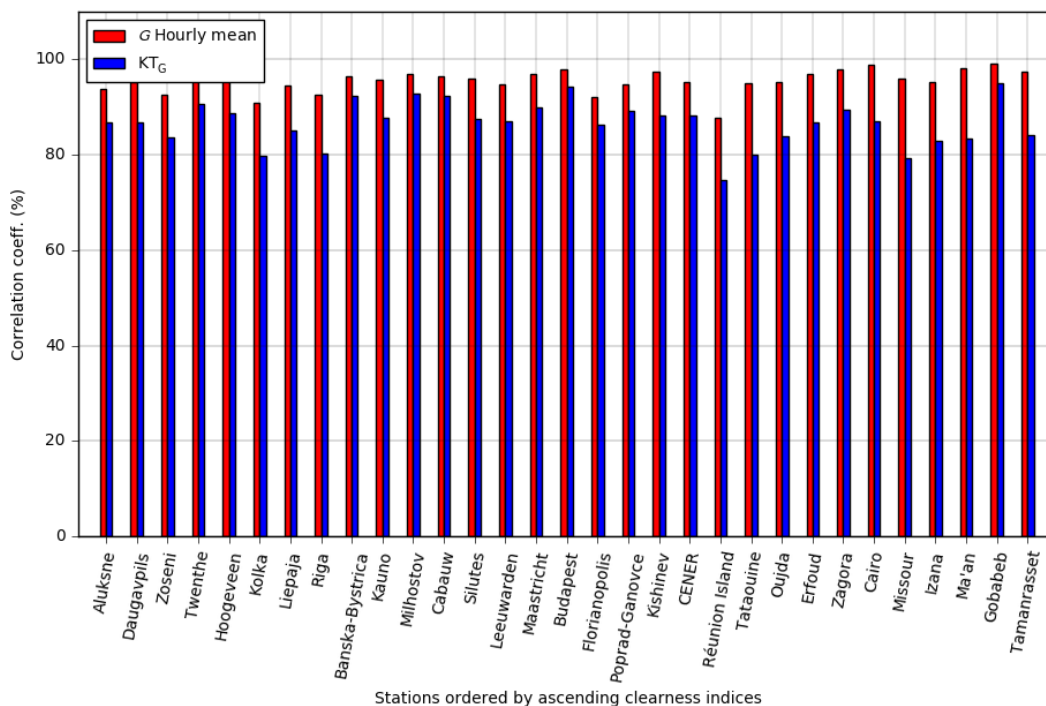
Figure 3.4. Correlation coefficients for global irradiance and clearness index.
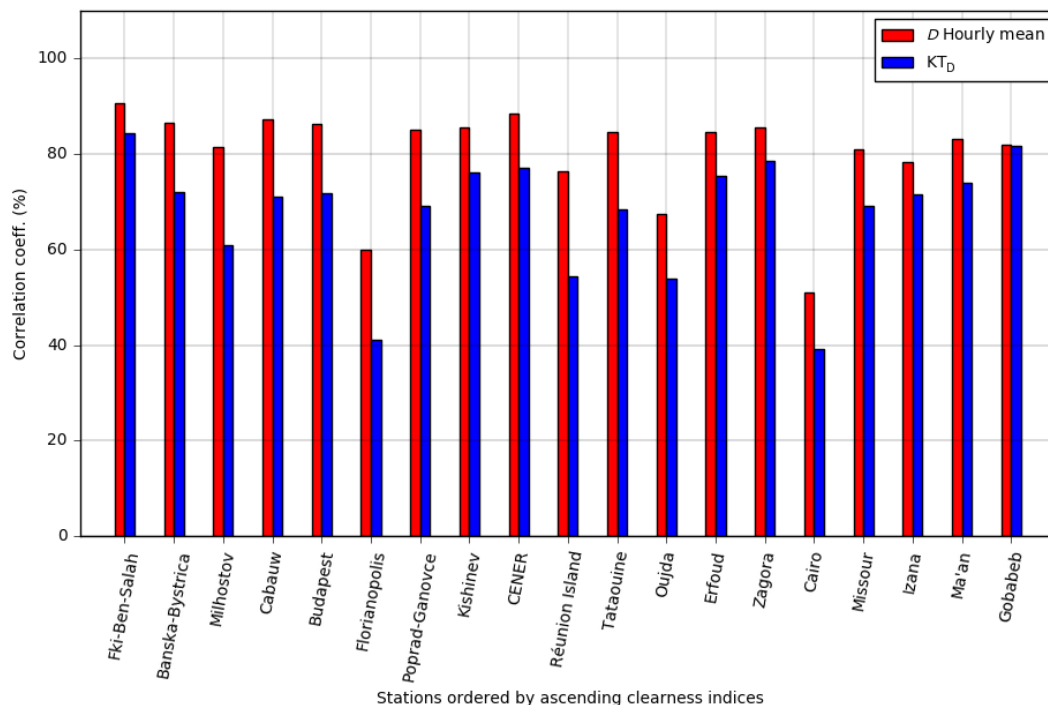
Figure 3.5. Correlation coefficients for diffuse irradiance and clearness index.
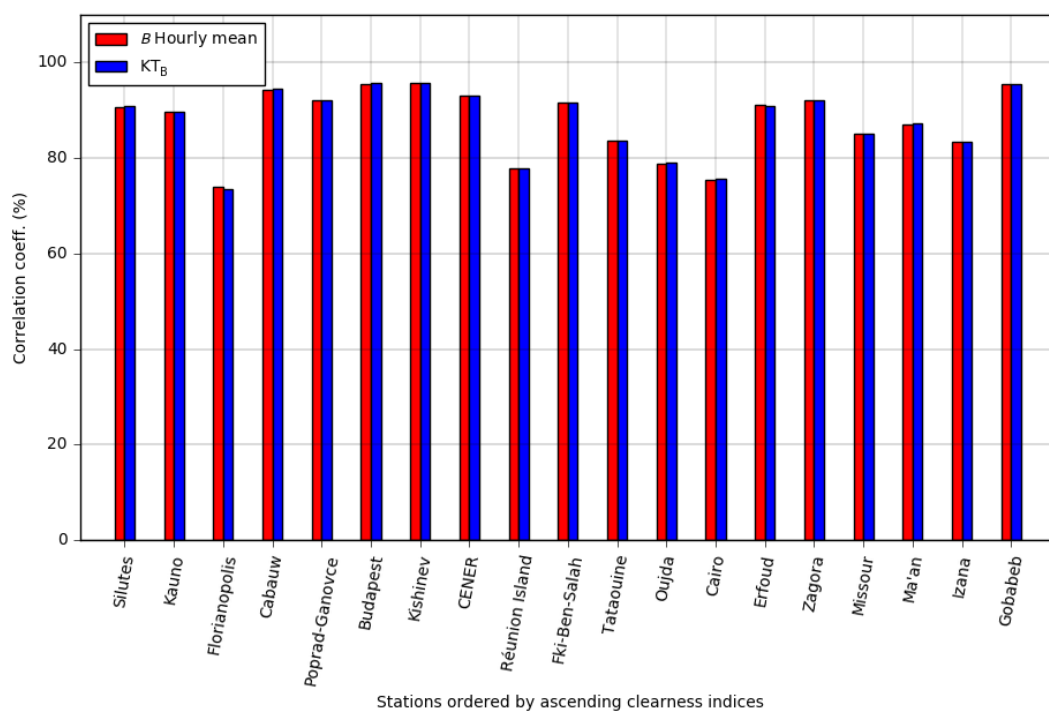
Figure 3.6. Correlation coefficients for direct normal irradiance and clearness index.

3.3 Ability to reproduce the frequency distributions of measurements

The frequency distributions of G and KT_G (Fig. 3.7 and 3.8), D and KT_D (Fig. 3.9 and 3.10), B and KT_B (Fig. 3.11 and 3.12) are given for several classes of irradiances or KT. The objective of these figures is to display in which bins of values an over- or underestimation of the frequencies may be observed.
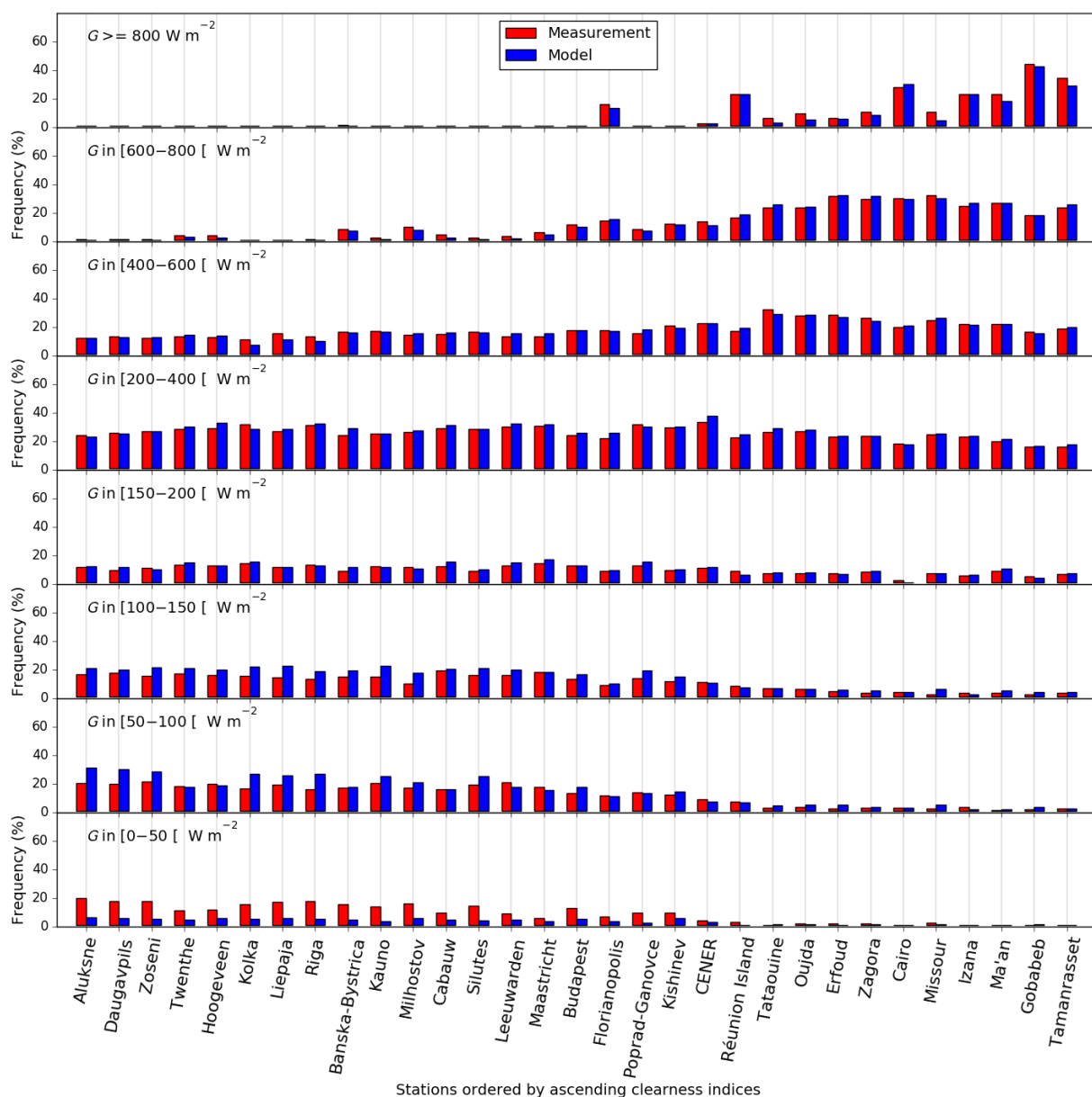
Figure 3.7. Frequency distribution of measurements for global irradiance.
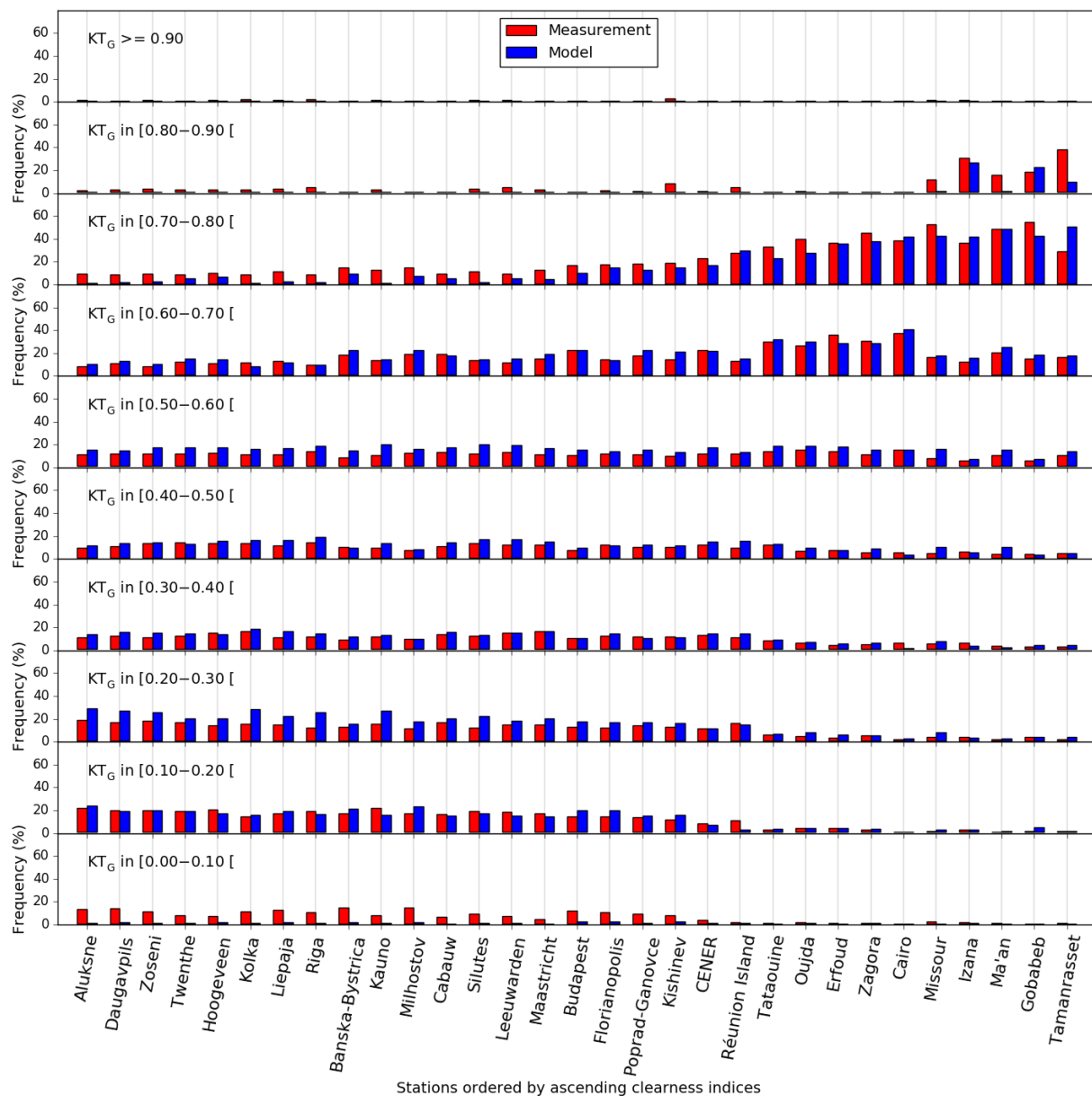
Figure 3.8. Frequency distribution of measurements for global clearness index.
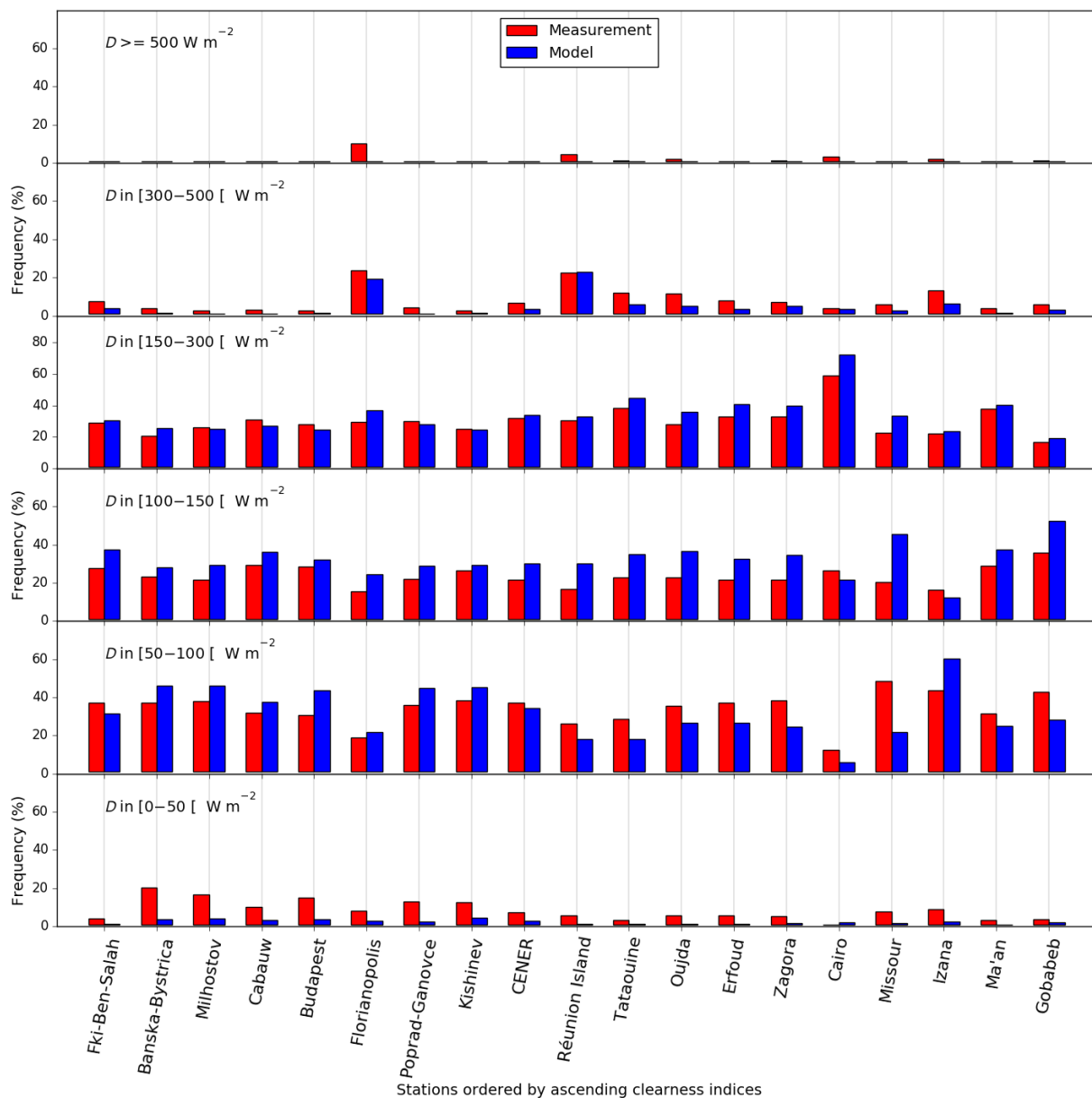
Figure 3.9. Frequency distribution of measurements for diffuse irradiances.
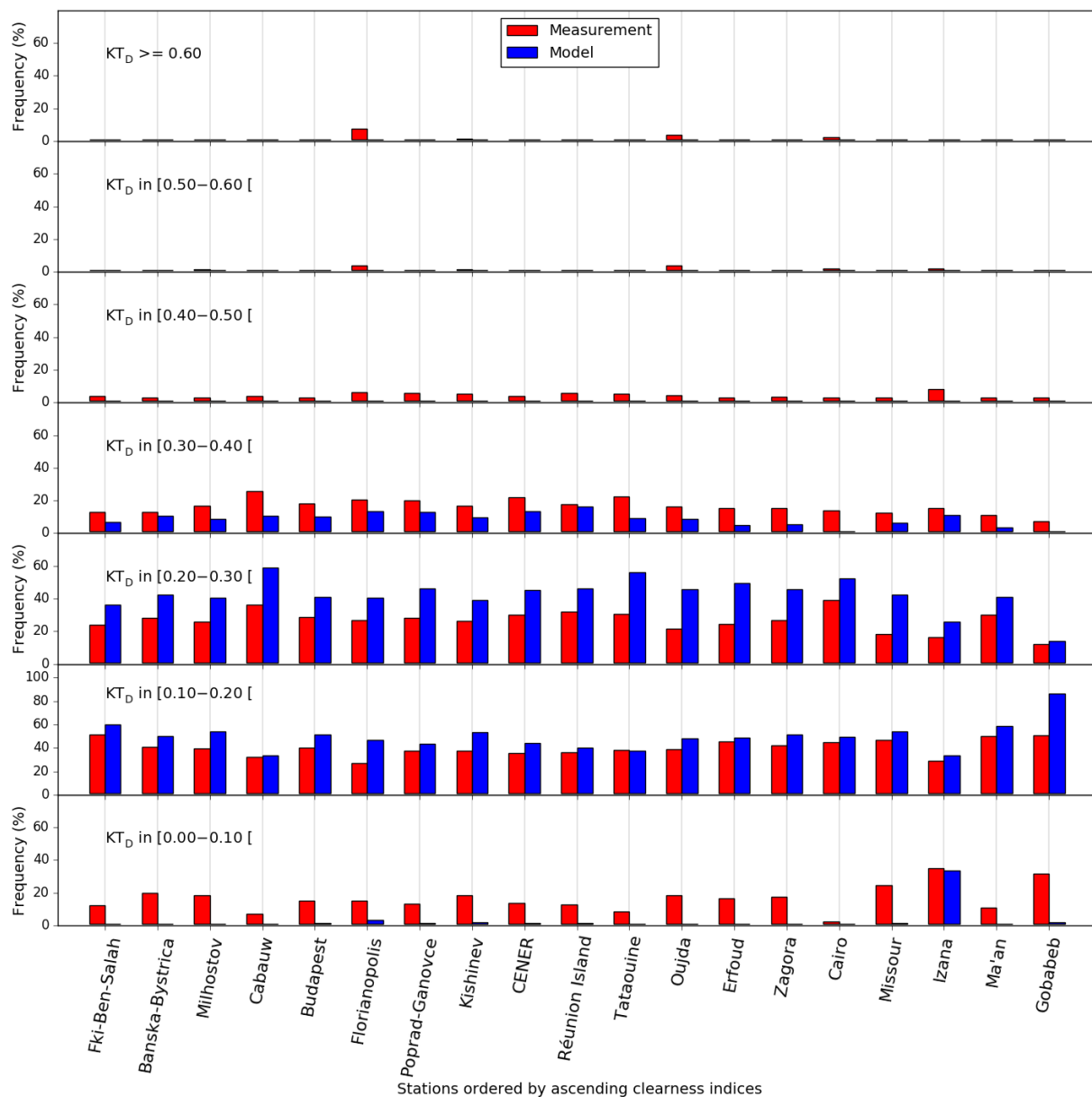
Figure 3.10. Frequency distribution of measurements for diffuse clearness index.
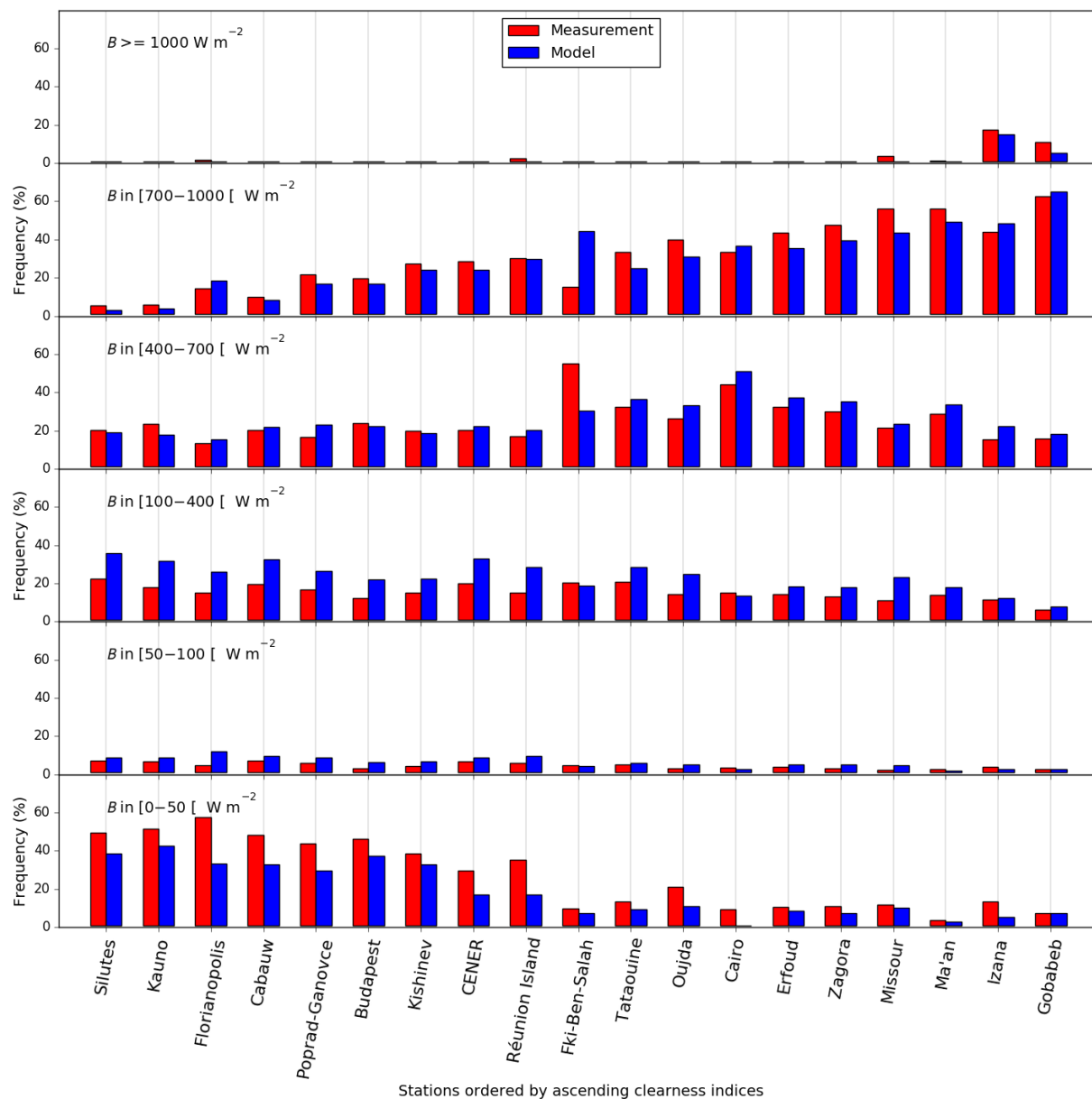
Figure 3.11. Frequency distribution of measurements for direct irradiances
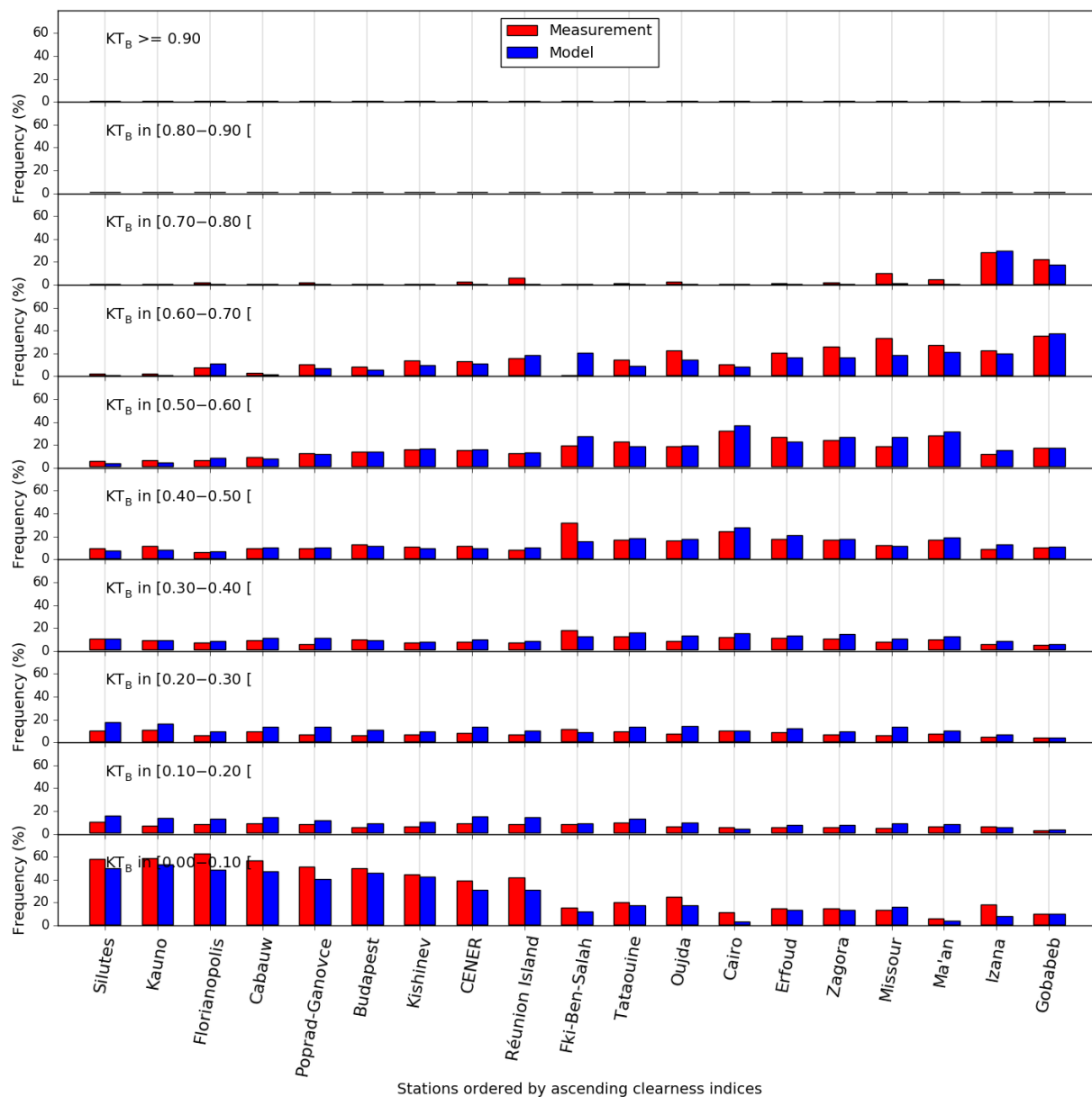
Figure 3.12. Frequency distribution of measurements for direct clearness index.

3.4 Ability to reproduce the monthly means and standard deviation for the period

The final batch of analyses deals with the capability of CRS to reproduce the monthly means of the irradiance for each month of the period and its variability within a month, expressed as the standard-deviation of the hourly values (estimates and observations) within this month. Figures 3.13 to 3.15 are respectively for *G*, *D* and *B*.
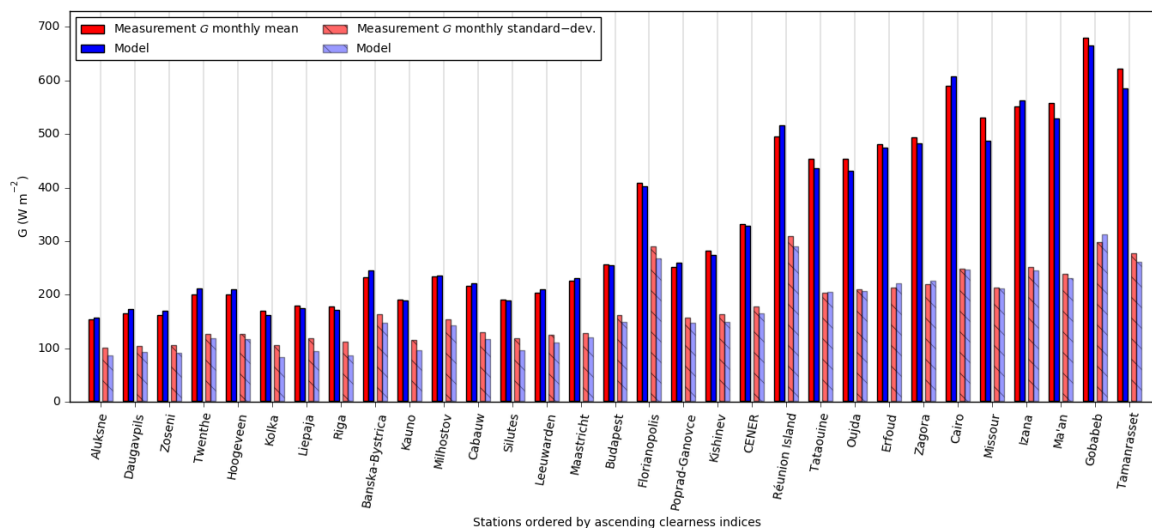
Figure 3.13. Monthly means and standard-deviations for global irradiance.
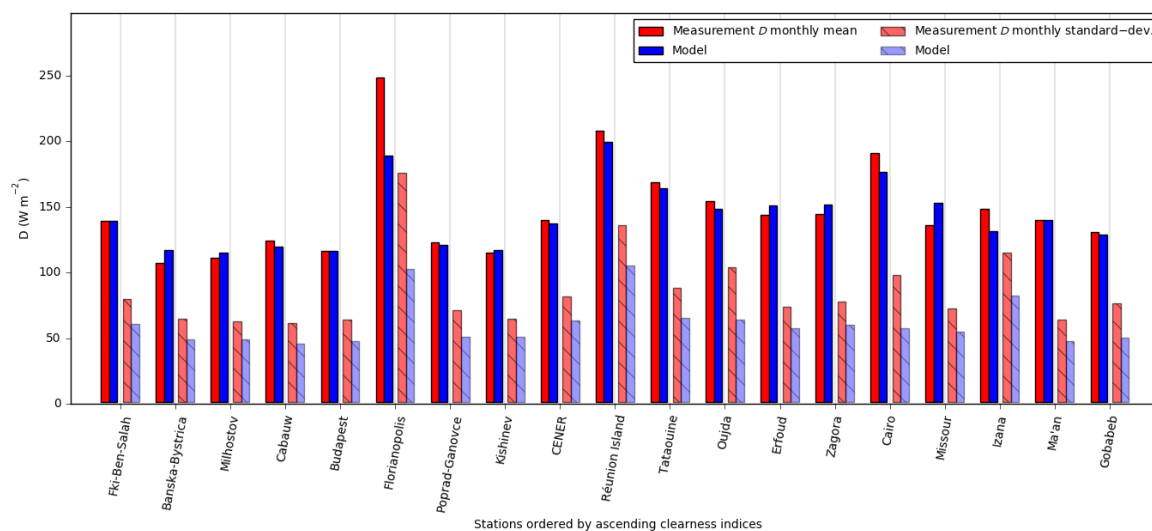
Figure 3.14. Monthly means and standard-deviations for diffuse irradiance.
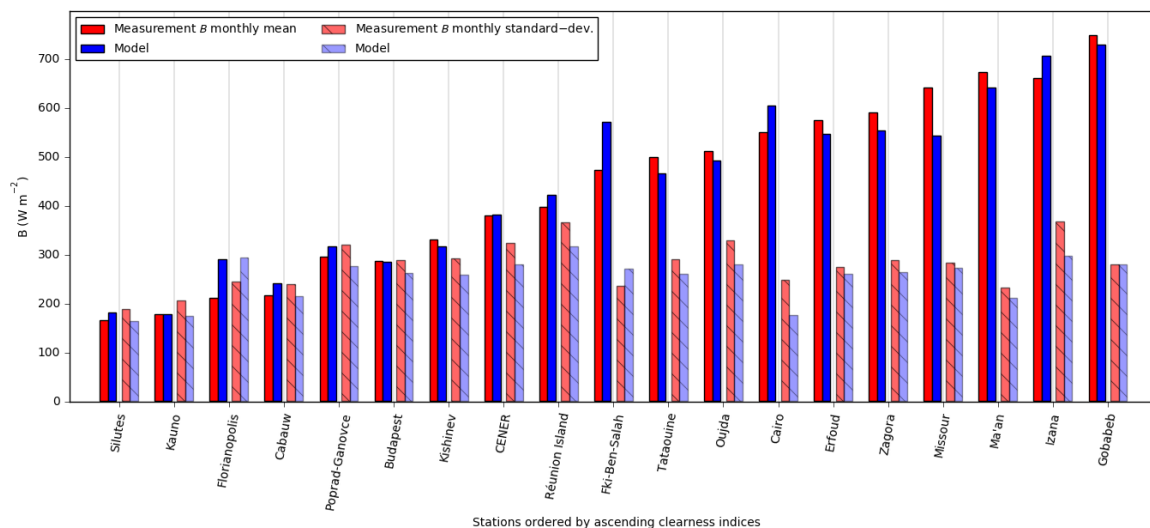
Figure 3.15. Monthly means and standard-deviation for direct normal irradiance.

3.5 Multi-annual statistical indicators

Statistical indicators (mean irradiance, mean KT, relative bias and relative RMSE) have been computed for the SON period and for the years 2016 to 2020. Figures 3.16 to 3.18 are respectively for *G*, *D* and *B*.

3.5.1 Global irradiance

CAMS-RAD Global horizontal irradiance

Mean values
from 2016 to 2020 (Sept.-Nov.)

Mean (W m^{-2})

	CY41R1 hires	CY43R1	CY45R1	CY46R1	CY47R1
		CY43R3			
Toravere (58.3°N)	199	169	203	204	
Kolka (57.7°N)				221	183
Aluksne (57.4°N)				226	181
Zoseni (57.1°N)	198	182	267	234	194
Riga (57.0°N)	213	171	206	220	196
Liepaja (56.5°N)	220	187	319	225	195
Daugavpils (55.9°N)		170	162	237	195
Silutes (55.4°N)	266	198	249	232	213
Kauno (54.9°N)		179	279	216	212
Leeuwarden (53.2°N)	267	227	251	233	227
Hoogeveen (52.8°N)	251	228	263	231	227
Twenthe (52.3°N)	247	223	263	228	226
Cabauw (52.0°N)	269	235	273	243	236
Maastricht (50.9°N)	269	240	275	241	245
Poprad-ganovce (49.0°N)	265	269	309	301	272
Banska-bystrica (48.7°N)	275	250	302	275	259
Milhostov (48.7°N)	264	256	294	289	252
Budapest (47.4°N)					271
Kishinev (47.0°N)	195	268	291	301	291
Payerne (46.8°N)	299	311	318	306	
Cener (42.8°N)	335	344	347	335	337
Oujda (34.6°N)	452	480	424	429	440
Tataouine (33.0°N)	430			464	438
Missour (32.9°N)	465	480		392	460
Erfoud (31.5°N)	492	494	478	496	477
Zagora (30.3°N)	486	501	514	497	486
Maan (30.2°N)	522	565	441	476	527
Cairo (30.0°N)	500	515	488	519	607
Izana (28.3°N)	584	580	580	598	570
Tamanrasset (22.8°N)	578	573	526	569	586
Florianopolis (27.6°S)	439	371	392	398	408
Gobabeb (23.6°S)	634	650	649	664	666
Reunion (20.9°S)					514

2016 SON — 2017 SON — 2018 SON — 2019 SON — 2020 SON

Scale: 550, 500, 450, 400, 350, 300, 250, 200, 150

CAMS-RAD Global horizontal irradiance

Mean clearness index values
from 2016 to 2020 (Sept.-Nov.)

Mean Kt

	CY41R1 hires	CY43R1	CY45R1	CY46R1	CY47R1
		CY43R3			
TORA	0.39	0.34	0.40	0.39	
KOLK				0.40	0.36
ALUK				0.41	0.35
ZOSE	0.38	0.34	0.48	0.42	0.37
RIGA	0.41	0.34	0.39	0.39	0.38
LIEP	0.41	0.36	0.48	0.40	0.37
DAUG		0.33	0.36	0.41	0.36
SILU	0.47	0.38	0.45	0.41	0.39
KAUN		0.34	0.48	0.39	0.39
LEEU	0.48	0.41	0.46	0.42	0.41
HOOG	0.45	0.40	0.47	0.41	0.41
TWEN	0.43	0.39	0.46	0.41	0.40
CABA	0.47	0.41	0.48	0.43	0.42
MAAS	0.45	0.41	0.48	0.42	0.42
POPR	0.44	0.45	0.52	0.50	0.46
BANS	0.45	0.42	0.50	0.45	0.43
MILH	0.43	0.42	0.48	0.47	0.41
BUDA					0.43
KISH	0.36	0.42	0.46	0.47	0.45
PAYE	0.47	0.50	0.50	0.48	
CENE	0.50	0.52	0.51	0.49	0.50
OUJD	0.59	0.63	0.56	0.56	0.57
TATA	0.55			0.59	0.56
MISS	0.59	0.64		0.56	0.60
ERFO	0.62	0.62	0.61	0.62	0.60
ZAGO	0.61	0.63	0.61	0.62	0.61
MAAN	0.66	0.69	0.59	0.65	0.66
CAIR	0.63	0.63	0.61	0.64	0.66
IZAN	0.71	0.70	0.71	0.73	0.69
TAMA	0.67	0.66	0.61	0.66	0.68
FLOR	0.46	0.43	0.41	0.41	0.42
GOBA	0.64	0.66	0.66	0.68	0.68
REUN					0.53

2016 SON — 2017 SON — 2018 SON — 2019 SON — 2020 SON
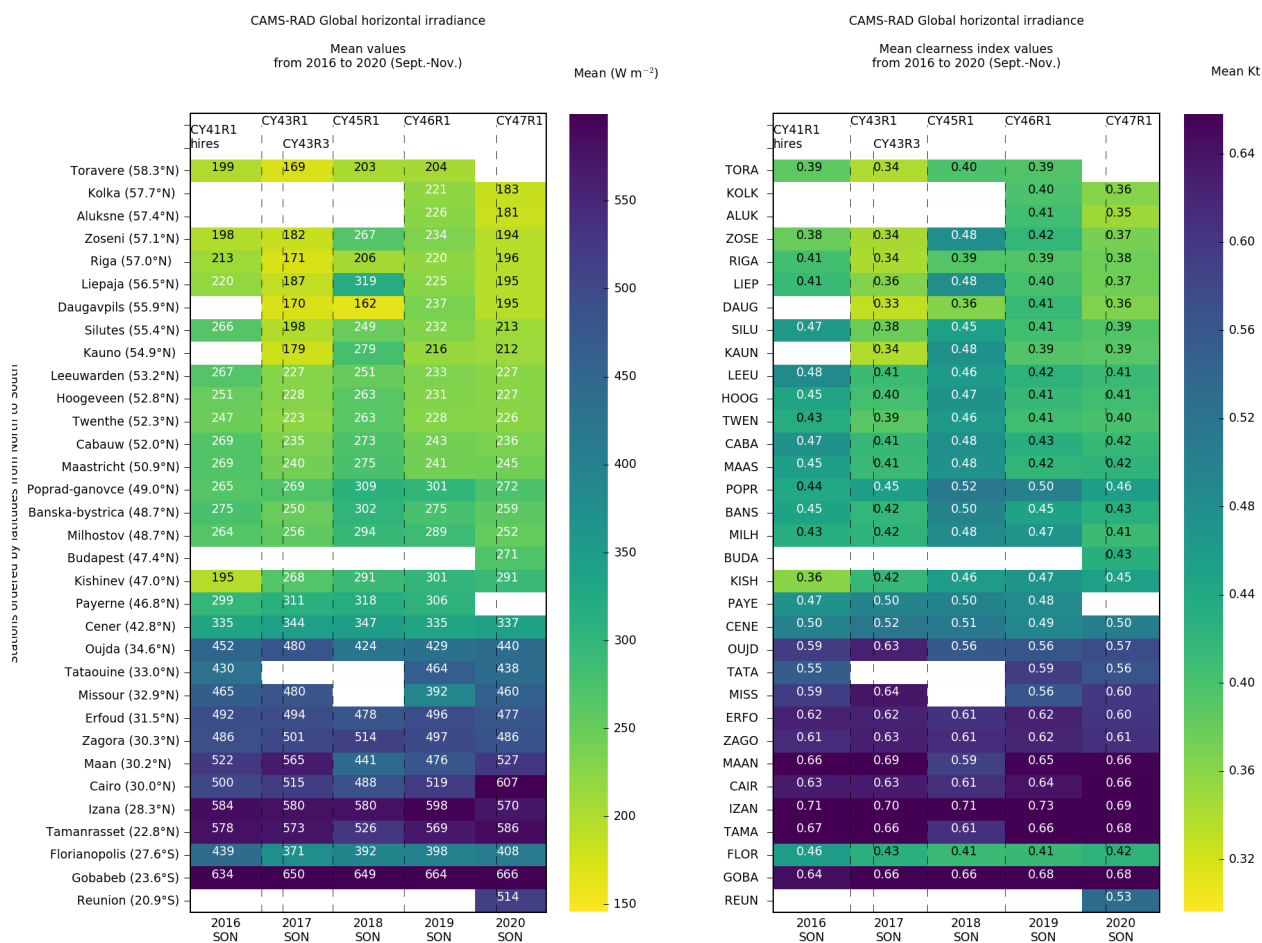
Scale: 0.64, 0.60, 0.56, 0.52, 0.48, 0.44, 0.40, 0.36, 0.32

Figure 3.16a. Multi-annual means for CAMS-RAD global horizontal
irradiance (left) and clearness index (right)
SON quarter from 2016 to 2020.

CAMS-RAD Global horizontal irradiance

Bias (relative to mean) quaterly performance
from 2016 to 2020 (Sept.-Nov.)

CAMS-RAD Global horizontal irradiance

RMSE (relative to mean) quaterly performance
from 2016 to 2020 (Sept.-Nov.)
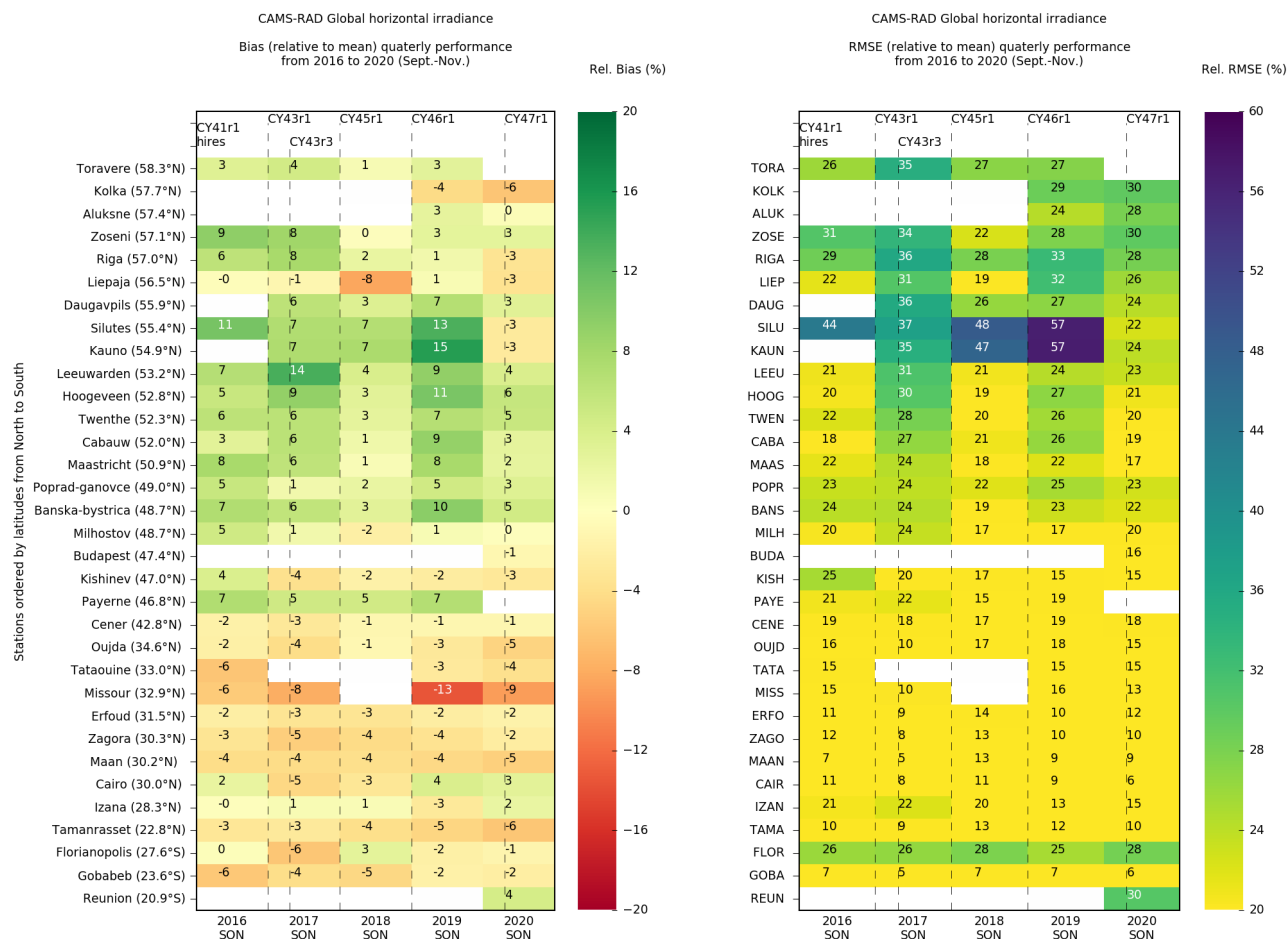
Figure 3.16b. Multi-annual relative bias (left) and relative RMSE (right)
for CAMS-RAD global horizontal irradiance
SON quarter from 2016 to 2020.
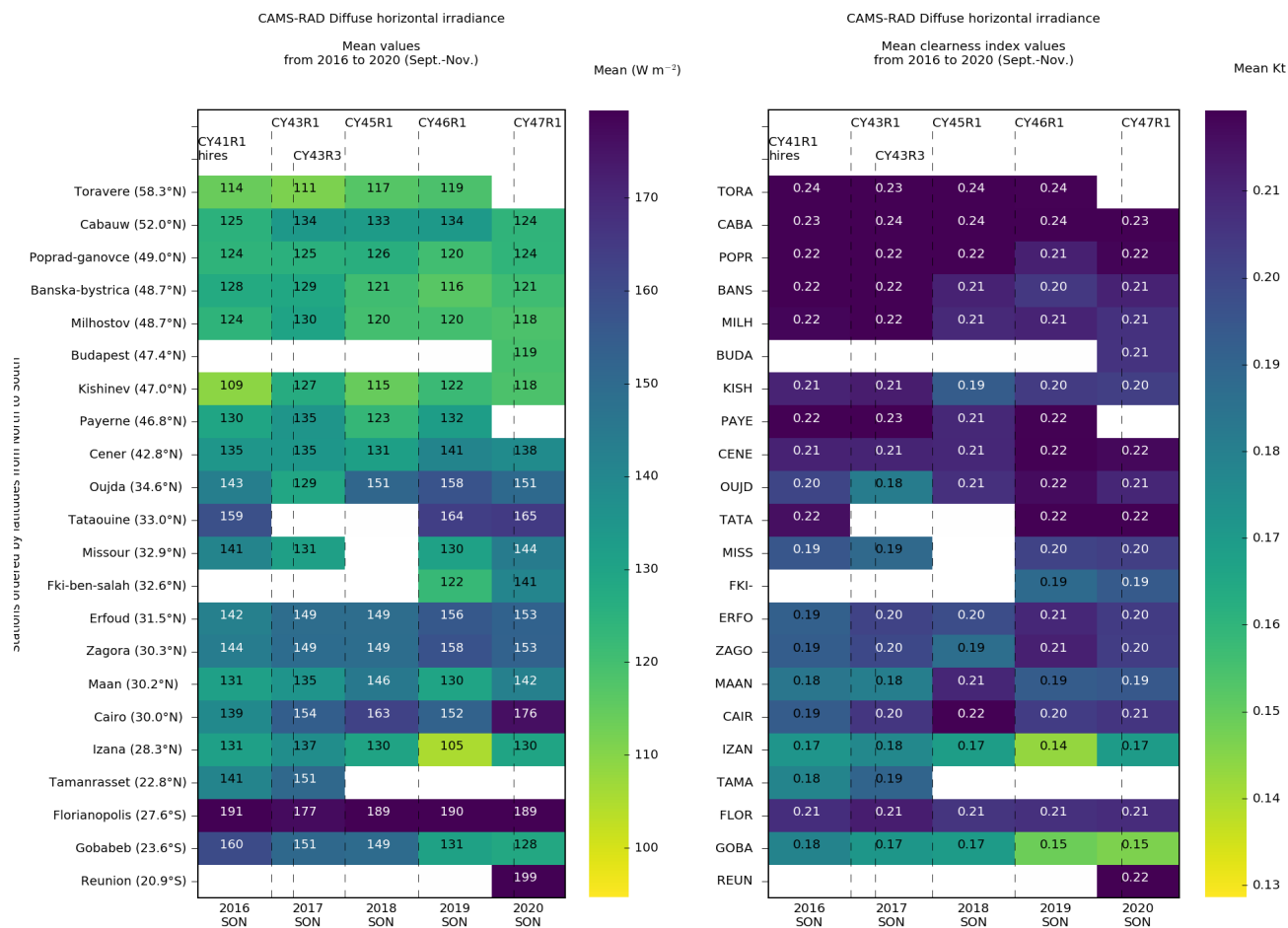
3.5.2 Diffuse irradiance

Figure 3.17a. Multi-annual means for CAMS-RAD diffuse horizontal
irradiance (left) and clearness index (right)
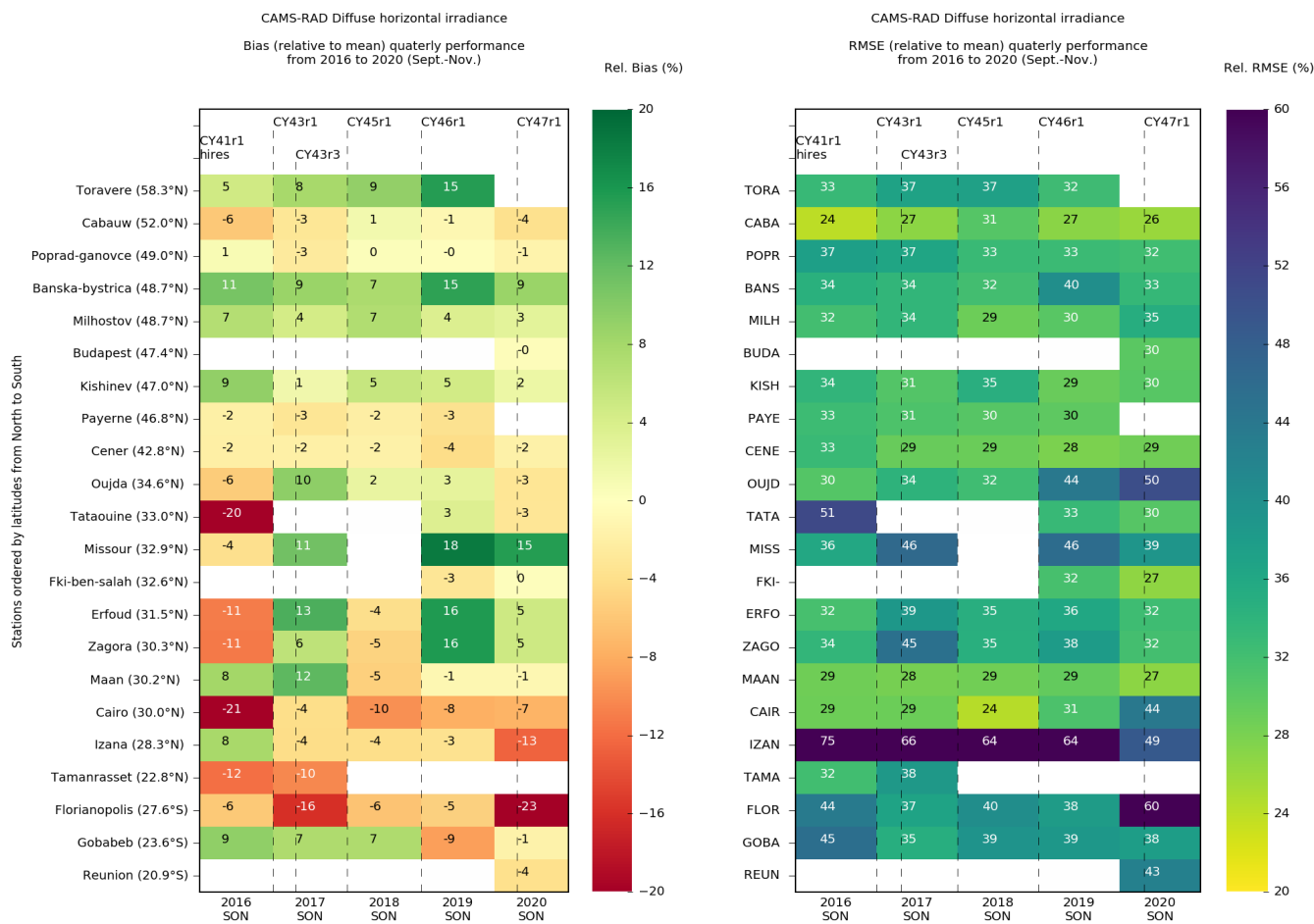SON quarter from 2016 to 2020.

Figure 3.17b. Multi-annual relative bias (left) and relative RMSE (right)
for CAMS-RAD diffuse horizontal irradiance.
SON quarter from 2016 to 2020.
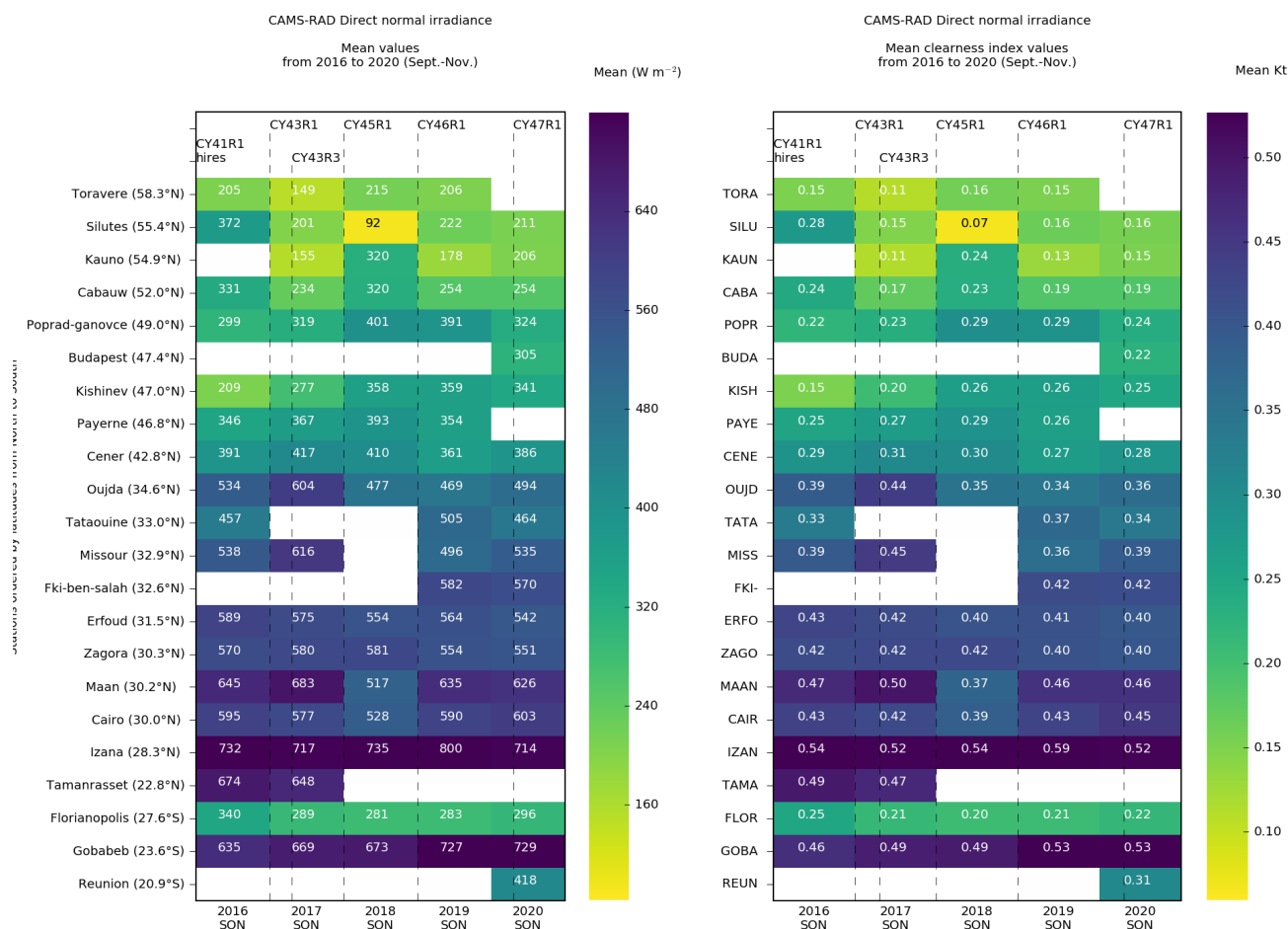
3.5.3 Direct normal irradiance

Figure 3.18a. Multi-annual means for CAMS-RAD direct normal
irradiance (left) and clearness index (right)
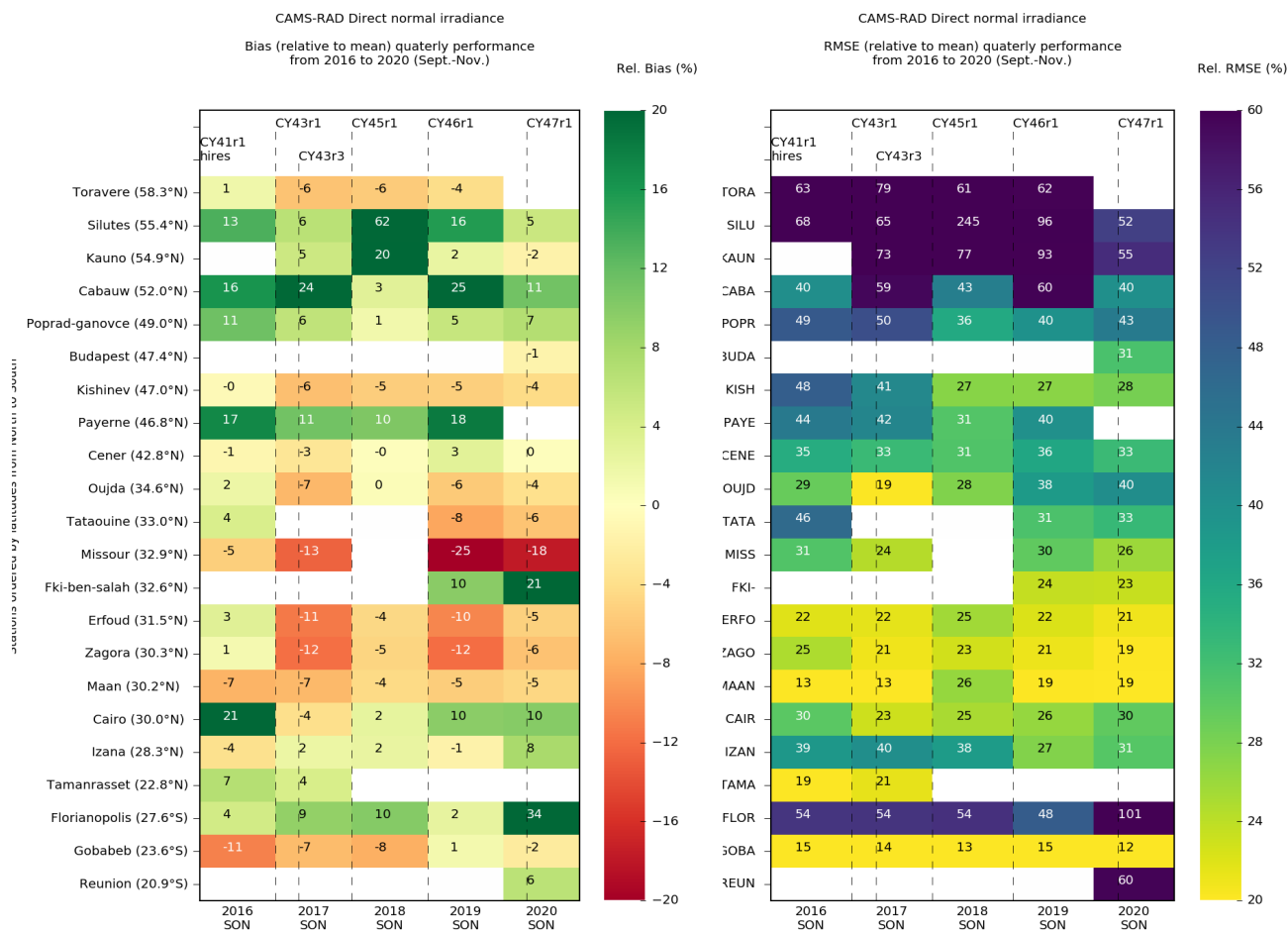SON quarter from 2016 to 2020.

CAMS-RAD Direct normal irradiance

Bias (relative to mean) quaterly performance
from 2016 to 2020 (Sept.-Nov.)

Rel. Bias (%)

Station	CY41r1 hires 2016 SON	CY43r1 / CY43r3 2017 SON	CY45r1 2018 SON	CY46r1 2019 SON	CY47r1 2020 SON
Toravere (58.3°N)	1	-6	-6	-4	
Silutes (55.4°N)	13	6	62	16	5
Kauno (54.9°N)		5	20	2	-2
Cabauw (52.0°N)	16	24	3	25	11
Poprad-ganovce (49.0°N)	11	6	1	5	7
Budapest (47.4°N)					-1
Kishinev (47.0°N)	-0	-6	-5	-5	-4
Payerne (46.8°N)	17	11	10	18	
Cener (42.8°N)	-1	-3	-0	3	0
Oujda (34.6°N)	2	-7	0	-6	-4
Tataouine (33.0°N)	4			-8	-6
Missour (32.9°N)	-5	-13		-25	-18
Fki-ben-salah (32.6°N)				10	21
Erfoud (31.5°N)	3	-11	-4	-10	-5
Zagora (30.3°N)	1	-12	-5	-12	-6
Maan (30.2°N)	-7	-7	-4	-5	-5
Cairo (30.0°N)	21	-4	2	10	10
Izana (28.3°N)	-4	2	2	-1	8
Tamanrasset (22.8°N)	7	4			
Florianopolis (27.6°S)	4	9	10	2	34
Gobabeb (23.6°S)	-11	-7	-8	1	-2
Reunion (20.9°S)					6

CAMS-RAD Direct normal irradiance

RMSE (relative to mean) quaterly performance
from 2016 to 2020 (Sept.-Nov.)

Rel. RMSE (%)

Station	CY41r1 hires 2016 SON	CY43r1 / CY43r3 2017 SON	CY45r1 2018 SON	CY46r1 2019 SON	CY47r1 2020 SON
TORA	63	79	61	62	
SILU	68	65	245	96	52
KAUN		73	77	93	55
CABA	40	59	43	60	40
POPR	49	50	36	40	43
BUDA					31
KISH	48	41	27	27	28
PAYE	44	42	31	40	
CENE	35	33	31	36	33
OUJD	29	19	28	38	40
TATA	46			31	33
MISS	31	24		30	26
FKI-				24	23
ERFO	22	22	25	22	21
ZAGO	25	21	23	21	19
MAAN	13	13	26	19	19
CAIR	30	23	25	26	30
IZAN	39	40	38	27	31
TAMA	19	21			
FLOR	54	54	54	48	101
GOBA	15	14	13	15	12
REUN					60

Figure 3.18b. Multi-annual relative bias (left) and relative RMSE (right)
for CAMS-RAD direct normal irradiance
SON quarter from 2016 to 2020.

3.6 Recommendations

As already reported in previous reports, there is room to improve the CRS for large solar zenithal angles. There are several cases with large B values observed in the ground observations which are underestimated in CRS. The cloud analysis from Meteosat images indicates a fully cloudy pixel with cloud coverage of 100 % and a low cloud optical depth. In the current scheme the cloud optical depth is set to a clipping value of 0.5 even if the retrieval provides a smaller value. This was a meaningful setting for the original application field of the used cloud retrieval package, but is not appropriate for surface radiation calculations. The exact value of the cloud optical depth plays a greater role when the sun is low above horizon which happens very often in winter at great

latitude, and at the beginning and end of the day in any case. This clipping value will be removed in the next version of the cloud retrieval package.

The CRS is composed of two models (see https://atmosphere.copernicus.eu/solar-radiation and the User Guide published there). The sky model of the CRS - called McClear - exploits the CAMS service information on aerosol properties and total column content in water vapour and ozone. It provides irradiances that would be observed in cloud-free conditions. McClear generally performs well as shown by several publications (Eissa et al., 2015; Lefèvre et al., 2013, Lefèvre, Wald, 2016; Marchand et al., 2017). However, detailed analyses of the deviations for CRS reveal discrepancies that may be large also for cloud-free cases. These discrepancies may be traced back to the over- or underestimation of the occurrences of cloud-free cases or to any gross errors in aerosol conditions modelled as input to McClear. Note should be taken that there is no means in this study to discriminate the cases of underestimation of the occurrences of overcast cases and those of underestimation of the optical depth. Both cases appear as an underestimation by CRS of the frequency of low clearness indices. Similarly, there is no means to discriminate the cases of overestimation of the occurrences of medium skies cases and those of underestimation of the optical depth of the optically thick clouds or overestimation of the optical depth of the optically thin clouds. These cases appear as an overestimation by CRS of the frequency of medium clearness indices. Finally, there is no means to discriminate the cases of underestimation of the occurrences of cloud-free cases and those of overestimation of the optical depth of the optically thin clouds. These cases appear as an underestimation by CRS of the frequency of large clearness indices.

4 Sources of data

Measurements are taken from various sources and measuring stations that are discussed in this section. Note that a more detailed presentation is done in the ground measurement catalogue updated every year: CAMS72_2018SC2_D72.1.4.1-2021_ground_catalogue_202106.pdf for June 2021.

4.1 Sources of data

Efforts are made to build the quarterly validation reports with the same set of stations to better follow and monitor the quality of the irradiance products delivered by the CRS, though this is difficult as discussed later.

Measurements originate from different networks as reported in Table 4.1. They have been acquired in different time systems (UT: Universal Time, TST: True Solar Time, GMT: Greenwich Meridian Time). No change in time system is performed during this validation. The handling of the different time systems is described in the annex A describing the procedure for validation.

Table 4.1. Source of data for each station, time system and type of data (*G, B, D* stands respectively for global, direct at normal incidence and diffuse), ordered from North to South.

Station	Source of data	Time system	Initial summarization	Type of data acquired
Toravere	BSRN	UT	1 min	G B D
Aluksne	Latvian Environment, Geology and Meteorology Centre (LEGMC)	TST	1 h	G - -
Kolka				G - -
Dobele				G B -
Riga				G - -
Zoseni				G - -
Liepaja				G - -
Rucava				G - -
Daugavpils				G - -
Silutes	Lithuanian Hydrometeorological Service (LHMS)	UT	1 h	G B -
Kauno				
Leeuwarden	KNMI	UT	1 h	G - -
Hoogeveen				
Twenthe				
Maastricht				
Cabauw	BSRN	UT	1 min	G B D
Poprad-Ganovce	Slovak Hydrometeorological Institute (SHMI)	UT	1 min	G B D
Banska-Bystrica				G - D
Milhostov				G - D
Budapest	BSRN	UT	1 min	G B D
Kishinev	WRDC	GMT+2	1 h	G B D
Payerne	BSRN	UT	1 min	G B D
Izaña	BSRN	UT	1 min	G B D
Oujda	EnerMENA	UT	1 min	G B D
Tataouine		UT+1		
Fki-Ben-Salah		UT		
Missour		UT		
Erfoud		UT		
Cairo		UT+2		
Zagora		UT		
Ma'an		UT+2		
Tamanrasset	BSRN	UT	1 min	G B D
Reunion island				
Gobabeb				
Florianopolis				

4.2 Short description of the stations selected for the validation

The selected stations are located in Europe, Africa and South America (see maps in Figures 2.1). Their geographical coordinates are given in Table 4.2.

Table 4.2. List of stations used to realize the validation report in general, and their coordinates.

Country	Station	Latitude	Longitude	Elevation a.s.l. (m)
Estonia	Toravere	58.254	26.462	70
Latvia	Aluksne	57.440	27.035	197
Latvia	Kolka	57.743	22.584	30
Latvia	Zoseni	57.135	25.906	188
Latvia	Riga	56.951	24.116	6
Latvia	Dobele	56.620	23.320	42
Latvia	Liepaja	56.475	21.021	4
Latvia	Rucava	56.162	21.173	19
Latvia	Daugavpils	55.870	26.617	98
Lithuania	Silutes	55.352	21.447	5
Lithuania	Kauno	54.884	23.836	77
The Netherlands	Hoorn	53.393	5.346	0
The Netherlands	Leeuwarden	53.225	5.755	1
The Netherlands	Hoogeveen	52.750	6.575	16
The Netherlands	Twenthe	52.273	6.897	34
The Netherlands	Cabauw	51.972	4.927	-1
The Netherlands	Vlissingen	51.442	3.596	8
The Netherlands	Maastricht	50.906	5.762	114
United Kingdom	Camborne	50.217	-5.317	88
Slovakia	Poprad-Ganovce	49.035	20.324	709
Slovakia	Banska-Bystrica	48.734	19.117	427
Slovakia	Milhostov	48.663	21.722	105
Hungary	Budapest	47.4291	19.1822	139
Moldova	Kishinev	47.000	28.817	205
Switzerland	Payerne	46.815	9.944	491
France	Carpentras	44.083	5.059	100
Spain	PSA	37.091	-2.358	500
Spain	Izaña	28.309	-16.499	2373
Morocco	Oujda	34.650	-1.900	617
Morocco	Missour	32.860	-4.107	1107
Morocco	Fki-Ben-Salah	32.578	-6.622	485
Morocco	Erfoud	31.491	-4.218	859
Morocco	Zagora	30.272	-5.852	783
Egypt	Cairo	31.036	31.009	104
Tunisia	Tataouine	32.974	10.485	210
Jordan	Ma'an	30.172	35.818	1012
Algeria	Adrar	27.878	-0.270	262
Algeria	Tamanrasset	22.790	5.529	1385
France	Reunion island	-20.9014	55.4836	116
Namibia	Gobabeb	-23.561	15.042	407
Brazil	Florianopolis	-27.605	-48.523	11

The selected stations are located in several different climates as reported in Table 4.3. The description of climates is taken from the updated world map of the Köppen-Geiger climate

classification by Peel et al. (2007).

Table 4.3. List of climates and corresponding stations

Climate	Stations
As: Tropical savanna climate, dry summer	Reunion island
Dfa: Continental wet. Cold climate without dry season and hot summer	Poprad-Ganovce, Banska-Bystrica, Milhostov
Dfb: Continental wet. Cold climate without dry season and warm summer	Toravere, Zoseni, Riga, Dobele, Daugavpils, Liepaja, Aluksne, Kolka, Rucava, Silutes, Kauno, Kishinev, Budapest
Cfa: Temperate climate without dry season and hot summer	Florianopolis
Cfb: Temperate climate without dry season and warm summer	Hoorn, Hoogeveen, Twenthe, Cabauw, Leeuwarden, Maastricht, Vlissingen, Camborne, Payerne
Csa: Temperate climate with dry and hot summer	Oujda, Missour
Csb: Temperate climate with dry and warm summer (Mediterran climate)	Carpentras, PSA, Izaña
BWh: Arid and hot climate of desert type	Tataouine, Erfoud, Cairo, Zagora, Ma'an, Tamanrasset, Fki-Ben-Salah
BWk: Arid and cold climate of desert type	Gobabeb

Among the set of stations, are several stations, such as Toravere, which are at the edge of the field of view of the Meteosat Second Generation satellites and most likely at the edge of physical assumptions used when retrieving cloud properties. This validation is meant to include extreme cases into the station list.

One may note that though the validation aims at validating the variables *G*, *B*, and *D* delivered by the CRS, several stations are included that measure only the global irradiance *G*. They have been selected in order to check the spatial consistency of the quality of the CRS products within the same network and same climate. Figure 2.1 shows several groups of stations that are close to each other within the same climate: The Eastern Baltic area, The Netherlands, and Slovakia. One expects similar performances of CRS within a group.

It should be underlined that the validation process cannot be automated in its present form. Hence, the number of selected stations and the choice of these stations is a trade-off between the desire to cover as much as possible various climatic conditions and the amount of human resources available.

4.3 Evolution of the list of stations

The selection of the stations considers the results published in scientific journals or conferences. Several authors have compared McClear or CRS estimates to ground-based measurements. These publications are analyzed to see if there are differences in quality when compared to our own validations.

The conclusions of these analyses may have an impact on the choice and the number of stations selected for the quarterly validation. For example, if one or more authors report performances that are dissimilar to ours in geographical areas for which we do not have stations, we will make our best to obtain measurements from stations if they obey our constraints in quality and timely access. In another example, authors may have made in-depth studies of the performances of CRS in geographical areas where we have stations, such as the Netherlands where we are using several KNMI stations. Given this background, exploiting a single KNMI station may be sufficient now to monitor the performances of CRS in this area.

4.4 Stations under evaluation

Some stations providing unusual observations are commented below.
From the #28 issue, some issues are not commented anymore. It concerns (see #27 issue for details):
- The KNMI station of Hoorn was removed from the set used for the quarterly validation. This station will be reported in the next ground data catalogue for information and as a warning to users at the coastal limit.
- The enerMENA station of Missour which gave abnormal overestimated measurements of diffuse irradiances during April and June 2018. This station was under maintenance since then and resume on October 2019.

From this #31 issue, some other stations are not commented anymore (see #30 issue for details):
- The Lithuanian stations of Silutes and Kauno. Thanks to the renovation operated in January 2020, problems have been solved, included many times shifts.

Still under evaluation are stations Zagora, Erfoud and Oujda in Morocco, Cairo in Egypt. Some discrepancies between estimated CRS and measurements have been reported in previous reports. In this #32 issue, the BSRN station of Florianopolis is illustrated regarding its bad results for this SON 2020 quarter.

4.4.1 Cairo (Egypt)

During the past 2019 and 2020 quarters some bad values for the D and B components appeared at Cairo which were not eliminated with the quality check process. Contrary to the global irradiance, the diffuse and direct irradiances present very large variations in Feb.-June 2020 (Fig. 4.1). A tracker failure along with a lack of cleaning during failure period explain these anomalies which

disappear by mid-June. For the present SON quarter, only Sept. is provisioned, before a new tracking failure in October.
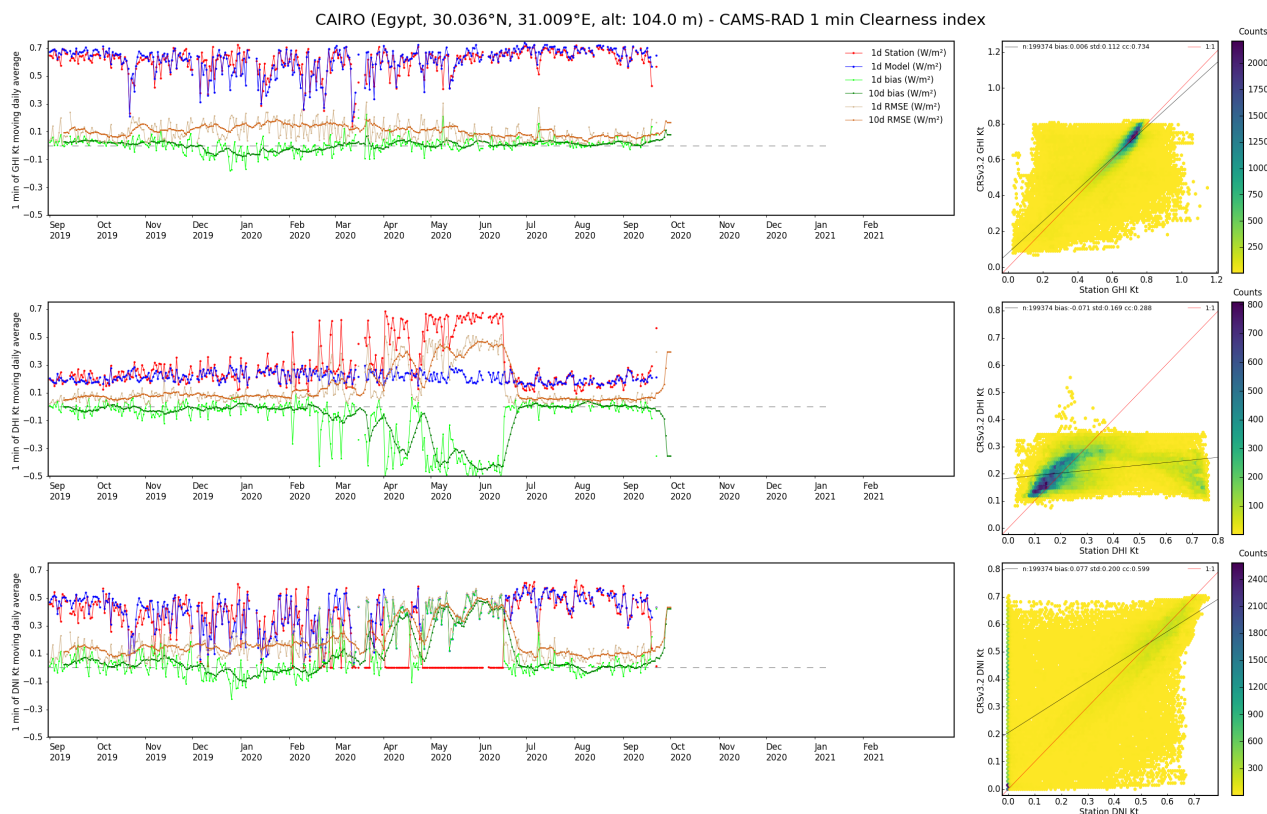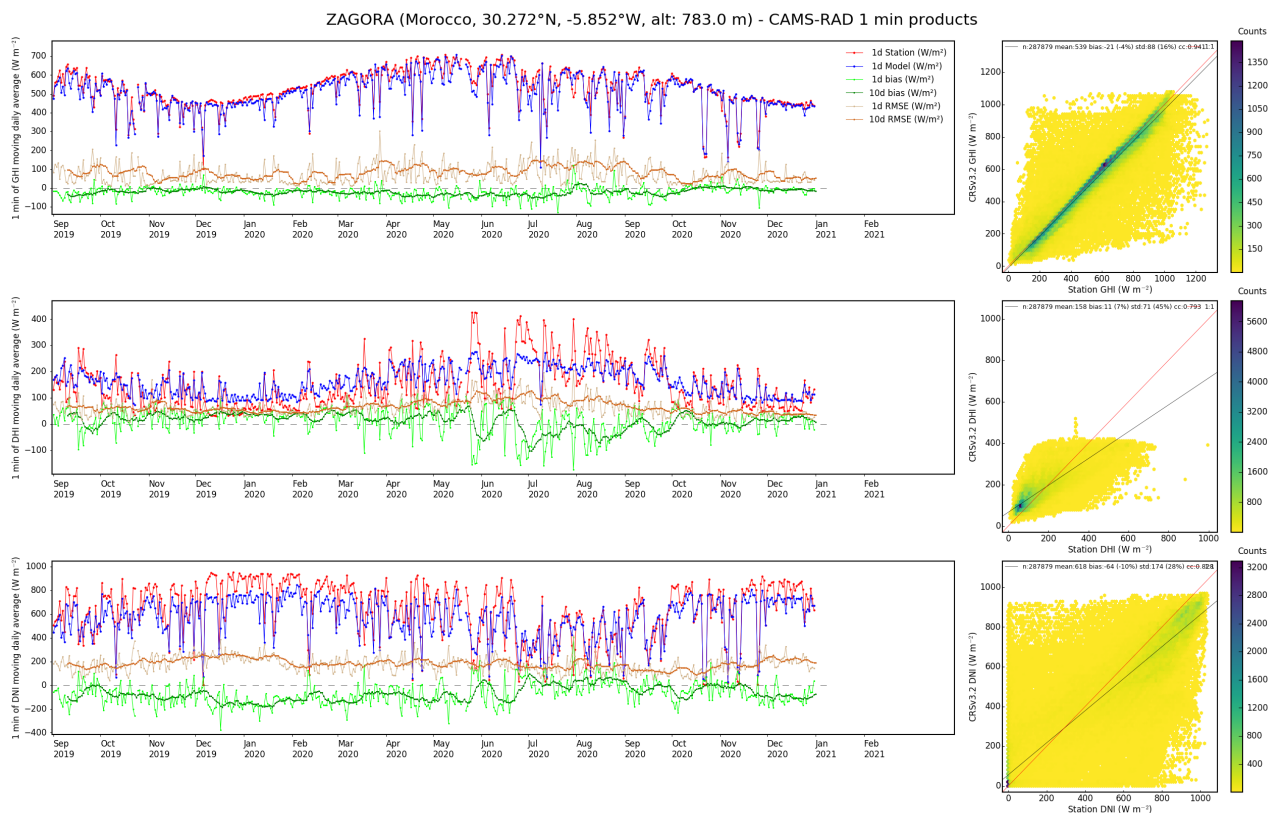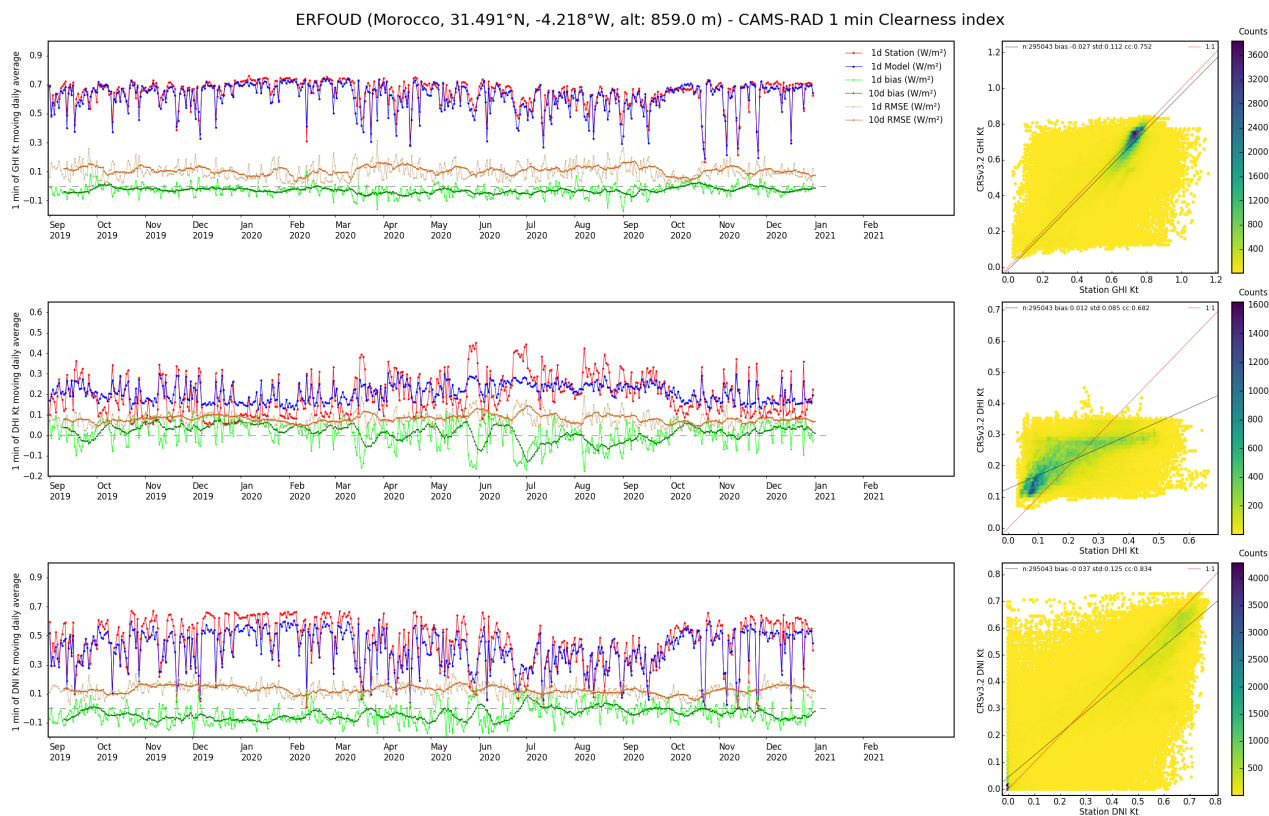

Figure 4.1. Station Cairo, daily and 10 days running average of clearness index during 2020.
from Sept. 2019 to Dec. 2020.
Top: Global. Middle: Diffuse. Bottom: Direct normal clearness index.

4.4.2 Zagora (Morocco)

The RSI sensor has been exchanged in January 2020. A new calibration has been applied that corrects the *G* component discrepancy between measured and estimated that was observed before. Nevertheless, *B* which is calculated from *G* and *D*, presents since then and until mid-June 2020 a discrepancy with estimated CRS that was not observed before. This discrepancy re-appears in October (Fig. 4.2).

Although large discrepancies appear during this SON 2020 period for the *D* and *B* components, no problem was reported regarding the maintenance of in-situ sensors. Thus, the data have not been eliminated from the SON 2020 dataset.
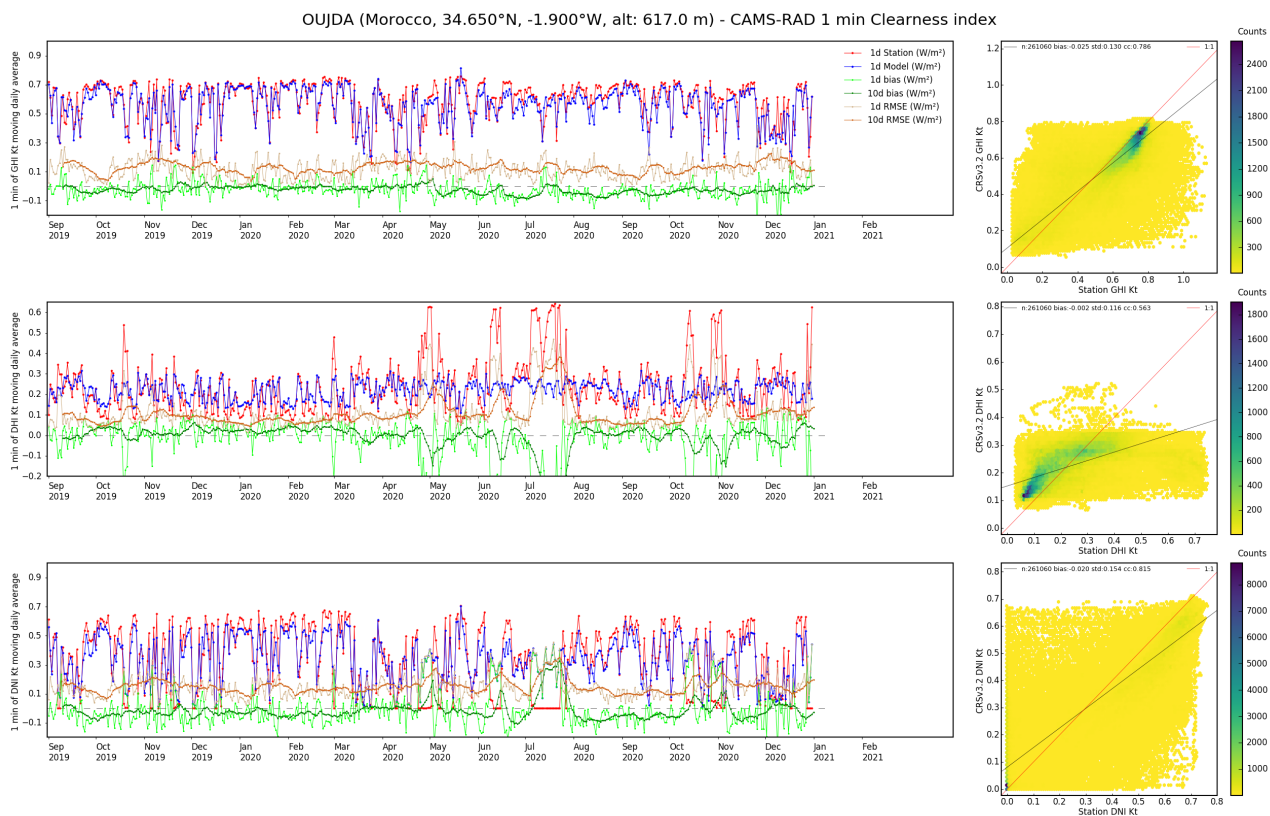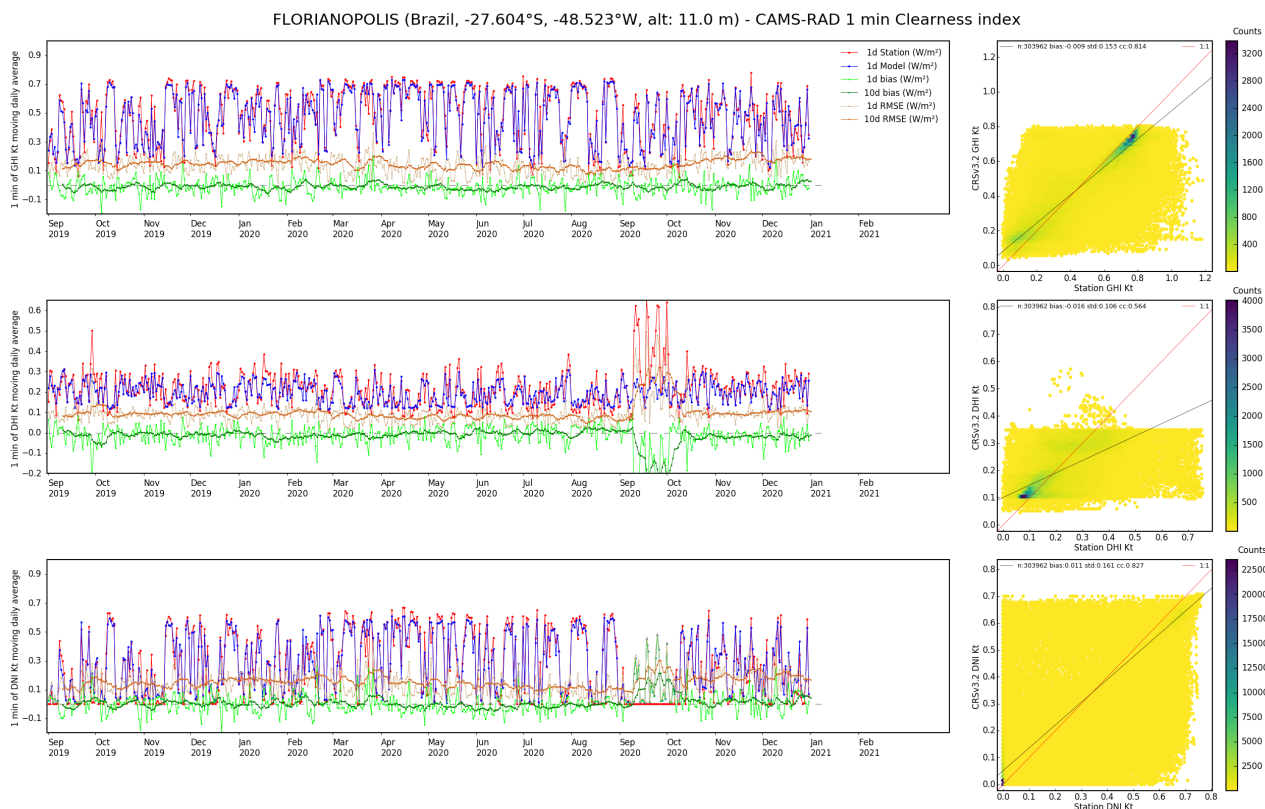
Figure 4.2. Station Zagora, daily and 10 days running average of clearness index
from Sept. 2019 to Dec. 2020.
Top: Global. Middle: Diffuse. Bottom: Direct normal clearness index.

4.4.3 Erfoud (Morocco)

The station Erfoud presents a decrease of *D* measurements from October 2019 to March 2020 and a sudden increase since then, with a concomitant variation of *B* in opposite way (Fig. 4.3). In this case of Erfoud, a remote site without regular cleaning, the continuously increasing deviations have been caused by dirt on the RSI sensor. Nevertheless, like Zagora, the discrepancies on *D* and *B* re-appear in October. Although large discrepancies appear during this SON 2020 period for the *D* and *B* components, no problem was reported regarding the maintenance of in-situ sensors. Thus, the data have not been eliminated from the SON 2020 dataset.

Figure 4.3. Station Erfoud, daily and 10 days running average of clearness index
from Sept. 2019 to Dec. 2020.
Top: Global. Middle: Diffuse. Bottom: Direct normal clearness index.

4.4.4 Oujda (Morocco)

Sensors were not cleaned during COVID-19 from March to May 2020, and a tracker failure occurred between 24 April and 3 May, and between 8-16 June which probably causes the discrepancy observed on the *D* component. Despite several tracker outages, no problem of maintenance was reported for SON 2020 although discrepancies remain. Thus, the data have not been eliminated from the SON 2020 dataset.

OUJDA (Morocco, 34.650°N, -1.900°W, alt: 617.0 m) - CAMS-RAD 1 min Clearness index

Figure 4.4. Station Oujda, daily and 10 days running average of clearness index
from Sept. 2019 to Dec. 2020.
Top: Global. Middle: Diffuse. Bottom: Direct normal clearness index.

4.4.5 Florianopolis (Brazil)

The BSRN station of Florianopolis exhibits unusual and large discrepancies during Sept. 2020 for the *D* and *B* components (Fig. 4.5).

Figure 4.5. Station Florianopolis, daily and 10 days running average of clearness index
from Sept. 2019 to Dec. 2020.
Top: Global. Middle: Diffuse. Bottom: Direct normal clearness index.

5 Acknowledgements

6 Reference documents

Blanc, P., Wald, L.: The SG2 algorithm for a fast and accurate computation of the position of the Sun. Solar Energy, 86, 3072-3083, doi: 10.1016/j.solener.2012.07.018, 2012.

Blanc, P., Espinar, B., Geuder, N., Gueymard, C., Meyer, R., Pitz-Paal, R., Reinhardt, B., Renne, D., Sengupta, M., Wald, L., Wilbert, S.: Direct normal irradiance related definitions and applications: the circumsolar issue. Solar Energy, 110, 561-577, doi: 10.1016/j.solener.2014.10.001, 2014.

Eissa, Y., Munawwar, S., Oumbe, A., Blanc, P., Ghedira, H., Wald, L., Bru, H., Goffe, D.: Validating surface downwelling solar irradiances estimated by the McClear model under cloud-free skies in the United Arab Emirates. Solar Energy, 114, 17-31, doi: 10.1016/j.solener.2015.01.017, 2015.

ISO Guide to the Expression of Uncertainty in Measurement: first edition, International Organization for Standardization, Geneva, Switzerland, 1995.

Greuell W., J. F. Meirink, and P. Wang (2013), Retrieval and validation of global, direct, and diffuse irradiance derived from SEVIRI satellite observations, J. Geophys. Res. Atmos., 118, 2340–2361, doi:10.1002/jgrd.50194.

Korany M., M. Boraiy, Y. Eissa, Y. Aoun, M. M. Abdel Wahab, S. C. Alfaro, P. Blanc, M. El-Metwally, H. Ghedira, K. Hungershoefer, Wald, L.: A database of multi-year (2004-2010) quality-assured surface solar hourly irradiation measurements for the Egyptian territory. Earth System Science Data, 8, 105-113, doi: 10.5194/essd-8-105-2016, 2016.

Lefèvre, M., Oumbe, A., Blanc, P., Espinar, B., Gschwind, B., Qu, Z., Wald, L., Schroedter-Homscheidt, M., Hoyer-Klick, C., Arola, A., Benedetti, A., Kaiser, J. W., Morcrette, J.-J.: McClear: a new model estimating downwelling solar radiation at ground level in clear-sky condition. Atmospheric Measurement Techniques, 6, 2403-2418, doi: 10.5194/amt-6-2403-2013, 2013.

Lefèvre, M., Wald, L.: Validation of the McClear clear-sky model in desert conditions with three stations in Israel. Advances in Science and Research, 13, 21-26, doi: 10.5194/asr-13-21-2016, 2016.

Marchand, M., Al-Azri, N., Ombe-Ndeffotsing, A., Wey, E., Wald, L.: Evaluating meso-scale change in performance of several databases of hourly surface irradiation in South-eastern Arabic Peninsula. Advances in Science and Research, 14, 7-15, doi:10.5194/asr-14-7-2017, 2017.

Peel, M. C., Finlayson, B. L., Mcmahon, T. A.: Updated world map of the Köppen-Geiger climate classification. Hydrol. Earth Syst. Sci. Discussions, 11(5), 1633-1644, 2007, hal-00305098.

WMO: Technical Note No. 172, WMO-No. 554, World Meteorological Organization, Geneva, Switzerland, 121-123, 1981.

WMO: Guide to meteorological instruments and methods of observation, WMO-No 8, 2008 edition updated in 2010, World Meteorological Organization, Geneva, Switzerland, 2012.

Annex A. Procedure for validation

The validation of a product is made by comparing high quality ground measurements acquired at a measuring station. These measurements are also called observations. There are several operations to perform *a)* to ensure that the observations are of sufficient quality so that they can be considered as a reference and *b)* to adapt the different time systems and samplings.

A.1 Controlling the quality of the observations and taking care of the time system

Time series of observation at stations have been screened for their quality according to the WMO procedure (1981) with details given in Korany et al. (2016). The automated procedure checks whether the observations exceed physically possible and extremely rare limits as well as tests of consistency between the various components of the radiation whenever possible and flags them as suspicious. Then an additional visual check is performed to further remove suspicious outliers.

Observations have been acquired in different time systems (UT: Universal Time, or TST: True Solar Time). No resampling of observations is performed in the procedure for validation. In the case of observations acquired in TST system, the procedure for collecting corresponding CRS data is as follows. Given the time stamp in TST, the times in UT for the beginning and the end of the observation are computed using the SG2 library (Blanc, Wald, 2012). In parallel, the CRS data are requested with a time step of 1 min in the UT system. The corresponding CRS irradiance is computed by summing up the 1 min data for the instants comprised between the two time limits.

A.2 Taking care of missing observations within an hour or one day

The validation may be performed at the sampling rate of the observations, e.g., every 1 min, 2 min, 10 min etc. It may be desirable to perform the validation at a time scale that is greater than the sampling rate, e.g. 1 h or 1 day. This necessitates summing up e.g. 60 observations at 1 min to yield the hourly irradiation.

Some of these observations will be flagged out by the quality check procedure. It comes out that some data is missing in a given hour and that the hourly irradiation cannot be computed with e.g. 60 observations made every 1 min within this hour but with less than 60. Hence, the sum of the valid observations is not the actual hourly irradiation; it will be equal or less.

One solution could be to reconstruct an hourly irradiation using e.g. the hourly profile of the extraterrestrial irradiation or of the irradiation in cloud-free case. This has been examined by the Task 36 "Solar Resource Knowledge Management" of the Solar Heating and Cooling Agreement of the International Energy Agency (2005-2010), which has recommended no to reconstruct hourly or daily irradiation from measurements with gaps.

The Task 36 has recommended instead constructing pseudo-hourly irradiation or irradiance by summing up the valid observations. A similar summation for the extraterrestrial irradiation is performed for exactly the same instants. This yields a pseudo-hourly extraterrestrial irradiation. The pseudo-hourly irradiation is valid only if the pseudo-hourly extraterrestrial irradiation is equal to or greater than 0.9 times the actual hourly extraterrestrial irradiation. This constraint is set to avoid extreme cases at sunrise and sunset. Invalid pseudo-hourly observations are rejected from the analysis. The same procedure applies to the daily irradiation if needed.

Pseudo-hourly irradiations from estimates are constructed in the same way.

A.3 Pairing observations and estimates

At that stage, two data sets are available. The first one contains original observations, or pseudo-hourly or pseudo-daily irradiations, depending on the case. Only valid observations have been retained. The second one is made of the original estimates, or pseudo-hourly or pseudo-daily irradiations, depending on the case. Only valid observations and estimates have been retained in these data sets.

For the sake of the simplicity, observations and estimates, respectively, will denote either the original observations and estimates, or the pseudo-hourly or pseudo-daily irradiations.

For each instant of valid observation, an observation is paired to the estimate from the product made at the location of the station and this instant. Only pairs are kept for the validation.

A.4 Overview of the procedure for validation

The procedure for validation comprises two parts. In the first one, differences between estimates and observations are computed and then summarized by classical statistical quantities. In the second part, statistical properties of estimates and observations are compared.

The procedure for validation applies to irradiation or irradiance, and clearness index. The changes in solar radiation at the top of the atmosphere due to changes in geometry, namely the daily course of the sun and seasonal effects, are usually well reproduced by models and lead to a de facto correlation between observations and estimates of irradiation. The clearness index is a stricter indicator of the performances of a model regarding its ability to estimate the optical state of the atmosphere. Though the clearness index is not completely independent of the position of the sun, the dependency is much less pronounced than for radiation.

A.5 Computation of deviations and statistical quantities

This part of the present protocol of validation puts one more constraint on observations.

Valid before 2020Q4 validation report (until DJF 2020):
Since the lowest values can be noise and are therefore insignificant in a validation process, any observation should be greater than a minimum significant value. If there are not, the observations, and the corresponding estimates, are removed from the data sets and are not kept for the computation of the deviations.

The threshold is selected in such a way such that there is a 99.7 % chance that the actual irradiance is significantly different from 0 and that it can be used for the comparison. It is set to 1.5 times the uncertainty of measurements of good quality as reported by the WMO (2012).

The threshold is 30 W m^{-2} (1.5 times 20 W m^{-2}) for the hourly (or intra-hourly) mean of global or diffuse irradiance and 7.5 W m^{-2} (1.5 times 5 W m^{-2}) for the daily mean of global or diffuse irradiance. As for the direct irradiance at normal incidence, the threshold was set to 22 W m^{-2} (1.5 times 15 W m^{-2}) for the hourly or intra-hourly mean and 7.5 W m^{-2} (1.5 times 5 W m^{-2}) for the daily mean.

December 2020 - change in the validation protocol on usage of lower thresholds:
From #30 report (MAM 2020 dataset) onwards, no threshold on irradiance value is applied to *B* anymore. A new threshold on solar elevation (>10°) is applied on all components in order to avoid horizon obstructions and directional response of pyranometers. This new protocol is based on a recent study comparing the effect of different thresholds on the validation. The results for the *B* component are presented in the report CAMS72_2018SC2_D72.1.6.1-2020, the Service update report 2020.
From this report #31 2021Q1 (JJA 2020 dataset) onwards, no threshold on irradiance value is applied to *G* and *D* anymore, in order to be consistent with *B*. The quality check procedure used to remove all *G* under 50 W m^{-2}, for the reason that under this value the tests cannot be performed. That also automatically removes *D* under 15 W m^{-2} approximately. Actually, it is unclear whether the data outside of the tested domain should be re-integrated into the dataset. A collaboration with the IEA PVPS task16 team for that (and other) unclear issues is foreseen. For the consistency of all components, the data outside the tested domain are re-integrated in the dataset.

Following the ISO standard (1995), the deviations are computed by subtracting observations for each instant from the estimates: deviation = estimate - observation. The set of deviations is summarized by a few quantities such as the bias or the root mean square error listed in next table. 2-D histograms between observations and estimates are drawn as well as histograms of the deviations.

Quantities summarizing the deviations

Mean of measurements at station kept for validation	The mean of the measurements made at the station and kept for validation for this period.
Number of data pairs kept for validation	The number of couples of coincident data (CRS, ground measurements) used for validation.
Percentage of data pairs kept relative to the number of original measurements	The number of couples of coincident data (CRS, ground measurements) kept divided by the number of measurements available and greater than 0 from the station.
Bias (positive means overestimation)	The mean error for the period, i.e. the mean of the deviations. It is also equal to the differences between the mean of the CRS product and the mean of the ground measurements. The bias denotes a systematic error. Ideal value is 0.
Bias relative to the mean of measurements	The bias divided by the mean of measurements kept for validation, expressed in per cent.
RMSE	The root mean square error. Deviations are squared then averaged, and the RMSE is the root of this average. Ideal value is 0.
RMSE relative to the mean of measurements	The RMSE divided by the mean of measurements kept for validation, expressed in per cent.
Standard deviation	The bias is subtracted from each deviation. The result is squared and averaged. The standard deviation is the root of this average. It denotes the scattering of the deviations around the bias. Ideally, the standard deviation of deviations must be close to 0, and more exactly within the standard deviation of the errors of the measurements.
Relative standard deviation	The standard deviation divided by the mean of measurements kept for validation, expressed in per cent.
Correlation coefficient	The correlation coefficient between the CRS data and the ground measurements. It denotes how well the CRS product reproduces the change in measurements with time. The closer to 1 the correlation coefficient, the better the reproduction of the variability.

Formula to compute the above-mentioned quantities

Formula

At instant k, observation is x_k and estimate (model) is y_k

Number of samples	N pairs of coincident values (x_k, y_k)
Mean observed value	$m_x = \frac{1}{N} \sum_{k=1}^{N} x_k$
Mean of the estimates y	$m_y = \frac{1}{N} \sum_{k=1}^{N} y_k$
Deviation at k	$\delta_k = (y_k - x_k)$
Bias (mean deviation, systematic error)	$b = \frac{1}{N} \sum_{k=1}^{N} \delta_k$
Relative bias	$rb = b/m_x$
Root mean square error	$RMSE = \sqrt{\frac{1}{N} \sum_{k=1}^{N} \delta_k^2}$
Relative RMSE	$rRMSE = RMSE/m_x$
Standard deviation of δ	$\sigma = \sqrt{\frac{1}{N} \sum_{k=1}^{N} (\delta_k - b)^2}$
Relative standard deviation	$r\sigma = \sigma/m_x$
Relation between b, $RMSE$ and σ	$RMSE^2 = b^2 + \sigma^2$
Standard deviation of x	$\sigma_x = \sqrt{\frac{1}{N} \sum_{k=1}^{N} (x_k - m_x)^2}$
Standard deviation of y	$\sigma_y = \sqrt{\frac{1}{N} \sum_{k=1}^{N} (y_k - m_y)^2}$
Covariance of x and y	$\sigma_{xy} = \frac{1}{N} \sum_{k=1}^{N} (x_k - m_x)(y_k - m_y)$
Correlation coefficient	$CC = \sigma_{xy}/\sigma_x \sigma_y$

Assuming that the observations achieve the "moderate quality" pyranometer measurements defined by WMO (2008, rev. 2012) for hourly global radiation, one may ask if the CRS estimates are compliant with "moderate quality". Defined as the 95 % probability (P95), the relative uncertainty for "moderate quality" should not exceed 20 %. The total uncertainty takes into account the uncertainty of observations and the uncertainty of the estimates. It can be expressed in a first approximation as the quadratic sum of both uncertainties. As a consequence, the total relative uncertainty should not exceed 28 % (P95), or 14 % (P66) if the estimates were of "moderate" quality.

A.6 Typical uncertainty of measurements

The World Meteorological Organization (WMO, 2012) sets recommendations for achieving a given accuracy in measuring solar radiation. This document clearly states that "good quality measurements are difficult to achieve in practice, and for routine operations, they can be achieved only with modern equipment and redundant measurements." The following Tables report the

typical uncertainty (95 % probability) that can be read in the WMO document. Uncertainties are expressed in J m^{-2} in the original document. The following Tables report them in W m^{-2} also.

Table A.1. Typical uncertainty (95 % probability) of measurements made by pyranometers
(source: WMO 2012)

	Good quality	Moderate quality
Hourly irradiation	8 % if irradiation is greater than 0.8 MJ m^{-2}. Otherwise uncertainty is 0.06 MJ m^{-2}, i.e. 6 J cm^{-2}, or for irradiance approx. 20 W m^{-2}	20 % if irradiation is greater than 0.8 MJ m^{-2}. Otherwise uncertainty is 0.16 MJ m^{-2}, i.e. 16 J cm^{-2}, or for irradiance approx. 50 W m^{-2}
Daily irradiation	5 % if irradiation is greater than 8 MJ m^{-2}. Otherwise, uncertainty is set to 0.4 MJ m^{-2}, i.e. 40 J cm^{-2}, or for irradiance approx. 5 W m^{-2}	10 % if irradiation is greater than 8 MJ m^{-2}. Otherwise, uncertainty is set to 0.8 MJ m^{-2}, i.e. 80 J cm^{-2}, or for irradiance approx. 9 W m^{-2}

Table A.2. Typical uncertainty (95 % probability) of measurements made by pyrheliometers
(source: WMO 2012)

	High quality	Good quality
1 min irradiation	0.9 % 0.56 kJ m^{-2}, or approx. 9 W m^{-2}	1.8 % 1 kJ m^{-2}, or approx. 17 W m^{-2}
Hourly irradiation	0.7 % 21 kJ m^{-2}, or approx. 6 W m^{-2}	1.5 % 54 kJ m^{-2}, or approx. 15 W m^{-2}
Daily irradiation	0.5 % 200 kJ m^{-2}, or approx. 2 W m^{-2}	1.0 % 400 kJ m^{-2}, or approx. 5 W m^{-2}

A.7 Definitions of a few quantities in solar radiation

The hourly global irradiation $G_{energy}h$ is the amount of energy received during 1 h on a horizontal plane at ground level. It is also known as hourly global horizontal irradiation, or hourly surface solar irradiation. The hourly diffuse irradiation $D_{energy}h$ is the amount of energy received from all directions of the sky vault, except that of the sun, during 1 h on a horizontal plane at ground level, and the hourly direct (or beam) irradiation $B_{energy}h$ is the amount of energy received from the direction of the sun during 1 h on this horizontal plane.

The hourly global irradiation $G_{energy}h$ is the sum of $B_{energy}h$ and $D_{energy}h$:
$G_{energy}h = B_{energy}h + D_{energy}h$

The hourly mean of global irradiance Gh, respectively direct irradiance $B_{horizontal}$h and diffuse irradiance Dh, is equal to G_{energy}h, respectively B_{energy}h and D_{energy}h, divided by 3600 s. If the irradiation is expressed in Wh m^{-2}, then the dividing duration is not 3600 s, but 1 h, yielding irradiance in W m^{-2}.

The hourly mean of direct irradiance at normal incidence Bh is the irradiance received from the direction of the sun during one hour on a plane always normal to the direction of the sun. See Blanc et al. (2014) for more details on the definition of the direct irradiance at normal incidence and the incidence of the circumsolar radiation.

For the sake of simplicity, the notation h is abandoned in this text from now on. The hourly means of global and diffuse irradiances are noted G and D, and the hourly mean of the direct irradiance at normal incidence is noted B.

The hourly clearness index KT is defined as the ratio of G to the hourly extra-terrestrial irradiance $G0$: $KT = G / G0$. The extra-terrestrial irradiance is computed here by the means of the SG2 algorithm (Blanc, Wald, 2012). The direct clearness index and the diffuse clearness index are defined in a similar way. Because the ratio of the direct horizontal to the direct normal is equal to the cosine of the solar zenithal angle at both ground level and top of atmosphere, it comes that the direct clearness index is the same than the direct normal clearness index.

Annex B. Station validation reports for this quarter

The validation reports provide histograms of irradiances and clearness indices computed for both observations and CRS estimates, as well as monthly means and standard deviations of hourly means of irradiance for each month of the period.

This document only includes an example of the validation report for this quarter and for a single station (Cabauw). Similar reports for all stations listed in Table 2.1 are available in pdf format in the supplement zip archive:

CAMS72_2018SC2_D72.1.3.1-2021Q1_annexB_stationwise/
CAMS72_2018SC2_D72.1.3.1-2021Q1_annex_B_SON2020_STATIONNAME.pdf

Annex B. Station CABAUW

SOLAR RADIATION VALIDATION REPORT

CAMS Radiation Service (CRSv3.2) - Hourly Mean of Irradiance
Cabauw - The Netherlands
Latitude: 51.972°N; Longitude: 4.927°E; Elevation a.s.l.: -0.7 m
From 2020-09 to 2020-11

This document reports on the performance of the product CAMS Radiation Service (CRSv3.2) when compared to high quality measurements of solar radiation made at the station of Cabauw from 2020-09 to 2020-11 using a standard validation protocol.

Report generated on 2021-05-21

I. Summary of performance

*Summary of the performances of the CRSv3.2 product for Hourly
Mean of Irradiance at Cabauw*

	Global	Diffuse	Direct Normal	Unit
Mean of measurements at station kept for validation	230	129	229	W/m²
Number of data pairs kept for validation	728	728	728	
Percentage of data pairs kept relative to the number of data >0 in the period	100	100	100	
Percentage of data pairs kept relative to the number of valid instants in the period	100	100	100	%
Bias (positive means overestimation; ideal value is 0)	6	-5	25	W/m²
Bias relative to the mean of measurements	3	-4	11	%
RMSE (ideal value is 0)	45	34	95	W/m²
RMSE relative to the mean of measurements	19	26	40	%
Standard deviation (ideal value is 0)	44	34	92	W/m²
Relative standard deviation	19	26	42	%
Correlation coefficient (ideal value is 1)	0.964	0.873	0.944	

II. 2-D histograms (scatter density plots) - Histogram of deviations

The 2-D histogram, also known as scatter density plot, indicates how well the estimates given by CRSv3.2 match the coincident measurements on a one-to-one basis. Colors depict the number of occurrences of a given pair (measurement, estimate). In the following, yellow is used for the least frequent pairs, with blue for intermediate frequencies and blue for the highest-frequency pairs. Ideally, the dots should lie along the red line. Dots above the red line mean an overestimation. Dots below the red line denote an underestimation. The mean of the measurements, the bias, the standard-deviation and the correlation coefficient are reported. The blue line is the affine function obtained by the first axis of inertia minimizing the bias and the standard-deviation. Ideally, this line should overlay the red line. The blue line shows the trend in error when values are far off the mean of the measurements.
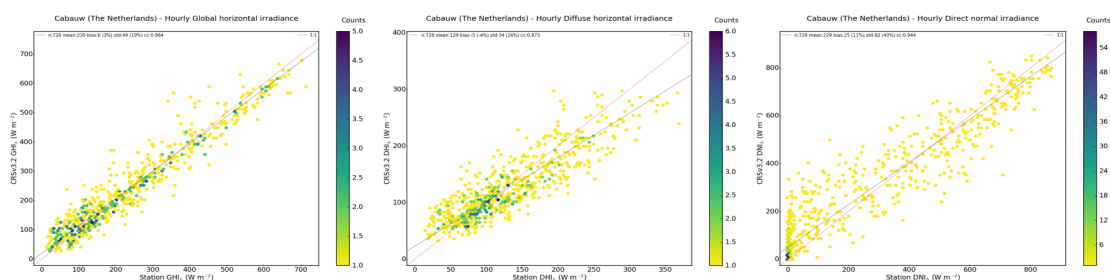

Figure 1. 2-D histogram between ground measurements (station) and the CRSv3.2 product for Hourly Mean of Irradiance

The histogram of the deviations, or as below the frequency distribution of the deviations, indicates the spreading of the deviations and their asymmetry with respect to the bias. Ideally, frequency should be 100% for deviation equal to 0. The more compact the frequency distribution of the deviations, the better.
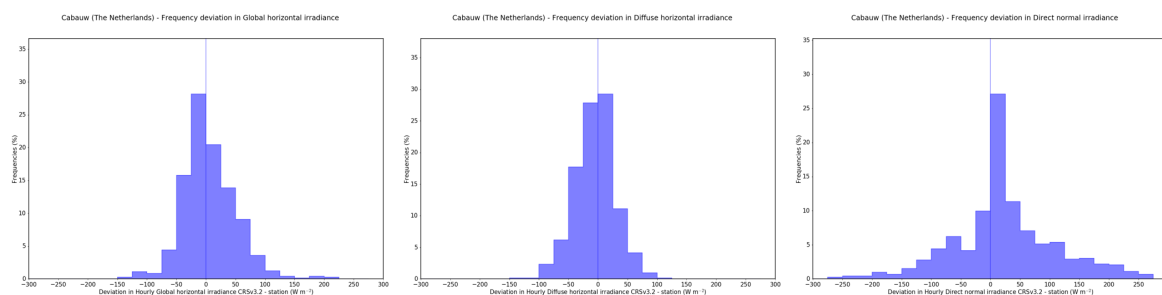

Figure 2. Frequency distribution of the deviations (CRSv3.2 - measurements)

III. Comparison of histograms

The graphs above deal with comparisons of measurements and CRSv3.2 values on a one-to-one basis: for each pair of coincident measurement and CRSv3.2 estimate, a deviation is computed and the resulting set of deviations is analysed.

This section deals with the statistical representativeness of the measurements by CRSv3.2. The frequency distributions of the measurements at station (red line) and the estimates (blue line) are computed and compared. A frequency distribution (histogram) shows how Hourly Mean of Irradiance values are distributed over the whole range of values. Ideally, the blue line should be superimposed onto the red one. If the blue line is above the red one for a given sub-range of values, it means that CRSv3.2 produces these values too frequently. Conversely, if the blue line is below the red one, CRSv3.2 does not produce values in this sub-range frequently enough.
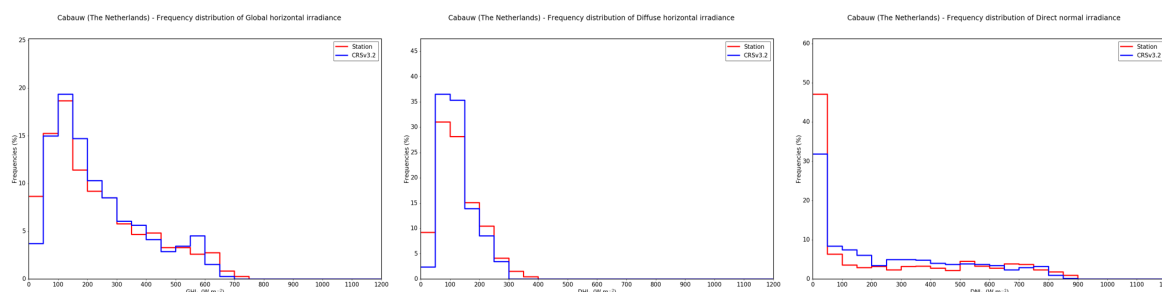

Figure 3. Frequency distributions of the measurements station (red line) and CRSv3.2 (blue line) for Hourly Mean of Irradiance

IV. Comparison of monthly means and standard deviations

For each calendar month (i.e., Jan, Feb, Mar...) in the selected period, all measurements kept for validation and the coincident CRSv3.2 estimates were averaged to yield the monthly means of Hourly Mean of Irradiance and the standard deviations. The standard-deviation is an indicator of the variability of the radiation within a month. In the following graph, monthly means are shown with diamonds and standard deviations as crosses. Red color is for measurements and blue color for CRSv3.2. The closer the blue symbols (CRSv3.2) to the red ones (measurements), the better. A difference between red dot (measurements) and blue diamond (CRSv3.2) for a given month denotes a systematic error for this month: underestimation if the blue diamond is below the red dot, overestimation otherwise. For a given month, a blue cross above the red one means that CRSv3.2 produces too much variability for this month. Conversely, CRSv3.2 does not contain enough variability in the opposite case.
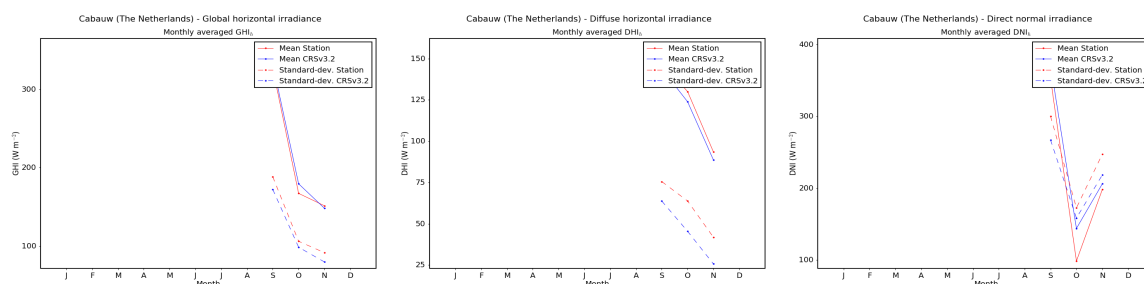

Figure 4. Monthly means of Hourly Mean of Irradiance measurements at station (red dots) and CRSv3.2 (blue diamonds), and monthly standard-deviation of measurements (red crosses) and CRSv3.2 (blue crosses)

V. Performances in clearness index

V.1. Summary of performances

Summary of the performance of the CRSv3.2 product for Hourly Mean of Clearness Index at Cabauw

	Global	Diffuse	Direct Normal	Unit
Mean of measurements at station kept for validation	0.406	0.238	0.168	
Number of data pairs kept for validation	728	728	728	
Percentage of data pairs kept relative to the number of data >0 in the period	100	100	100	
Percentage of data pairs kept relative to the number of valid instants in the period	100	100	100	%
Bias (positive means overestimation; ideal value is 0)	0.009	-0.009	0.019	
Bias relative to the mean of measurements	2	-4	11	%

RMSE (ideal value is 0)	0.083	0.065	0.070	
RMSE relative to the mean of measurements	20	27	40	%
Standard deviation (ideal value is 0)	0.083	0.064	0.067	
Relative standard deviation	21	27	41	%
Correlation coefficient (ideal value is 1)	0.923	0.711	0.944	

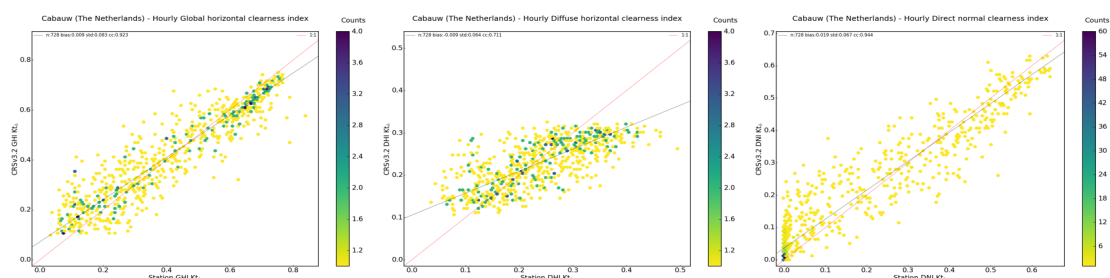## V.2. 2-D histograms (scatter density plots) - Comparison of histograms

Figure 5. 2-D histogram between ground measurements (station) and the CRSv3.2 product for Hourly Mean of Clearness Index
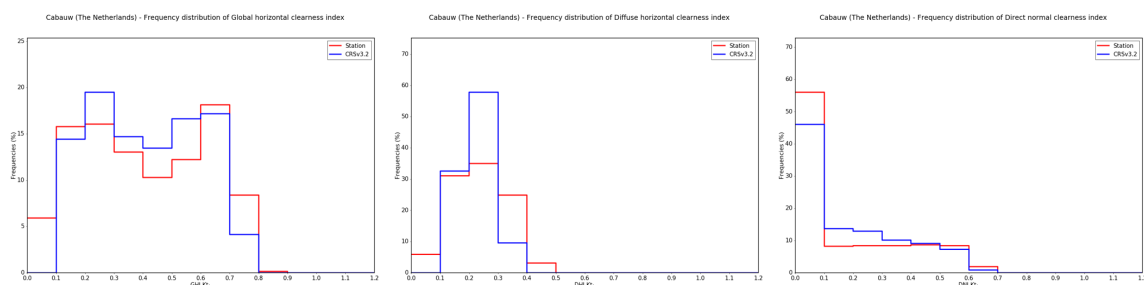

Figure 6. Frequency distributions of the measurements station (red line) and CRSv3.2 (blue line) for Hourly Mean of Clearness Index

Copernicus Atmosphere Monitoring Service

atmosphere.copernicus.eu   copernicus.eu   ecmwf.int